SYNTHESIS AND CHARACTERIZATION OF SILVER - ALUMINA NANOCOMPOSITES

A DISSERTATION

Submitted in partial fulfillment of the requirements for the award of the degree of

MASTER OF TECHNOLOGY

in

ADVANCED CHEMICAL ANALYSIS

By

RAVI KANT SHARMA

DEPARTMENT OF CHEMISTRY
INDIAN INSTITUTE OF TECHNOLOGY ROORKEE
ROORKEE - 247 667 (INDIA)

JUNE, 2012

CANDIDATE'S DECLARATION

I hereby declare that the work which is being presented in this dissertation entitled **"Synthesis and Characterization of Silver-Alumina Nanocomposites"** in partial fulfillment of the requirements for the award of the degree of **Master of Technology** in Chemistry with specialization in **"Advanced Chemical Analysis (A.C.A.)"**, and submitted in the **Department of Chemistry** at **Indian Institute of Technology Roorkee,** is an authentic record of the work carried out by me during the period August 2011 to June 2012, under the guidance of **Dr. P. Jeevanandam,** Assistant Professor, Department of Chemistry, Indian Institute of Technology Roorkee, Roorkee.

The matter presented in this dissertation work has not been submitted by me for the award of any other degree of this or any other Institute.

Date: June 2012

Place. ROORKEE

Ravi Kant Sharma

(RAVI KANT SHARMA)

CERTIFICATE

This is to certify that the above statement made by the candidate is correct to the best of my knowledge.

Anand 04/06/12

(Dr. P. Jeevanandam)
Assistant Professor
Department of Chemistry
Indian Institute of Technology Roorkee
ROORKEE-247667 (INDIA)

PREFACE

The work comprised in this thesis entitled "Synthesis and characterization of silver-alumina nanocomposites" consists of five Chapters, Introduction, Experimental details, Results and discussion, Summary and Future prospects are the Chapters 1, 2, 3, 4 and 5, respectively. A simple thermal decomposition approach has been used for the synthesis of silver-alumina nanocomposites. Two different supports, i.e. sol-gel alumina and commercial alumina (with/ without calcination) were used for the preparation of silver-alumina nanocomposites. The nanocomposites were characterized by powder X-ray diffraction, Fourier transform infrared spectroscopy, thermal gravimetric analysis, surface area measurements, field emission scanning electron microscopy coupled with energy dispersive X-ray analysis, transmission electron microscopy and diffuse reflectance spectroscopy.

ACKNOWLEDGEMENT

I wish to express my deepest gratitude and sincere thanks to my guide ***Dr. P. Jeevanandam****, Assistant Professor, Chemistry Department, Indian Institute of Technology Roorkee, for his valuable guidance, support and motivation to complete my dissertation work. The valuable hours of discussion and suggestions that I had with him have undoubtedly helped in supplementing my thoughts in the right direction for attaining the desired objectives. I consider myself extremely fortunate for having the opportunity to learn and work under his valuable supervision over the entire period of my association with him.*

I wish to express my sincere thanks to Dr. V. K. Gupta, Professor and Head, Department of Chemistry, Indian Institute of Technology Roorkee, Dr. R. K. Dutta, Coordinator of the M.Tech programme, for providing good infrastructure facilities and motivational support.

My sincere thanks to my lab mates Manu Sharma, Naga Ratna Kishore, Geetu Sharma, Nisha Bayal, Sudheer Kumar Yadav, Syam Kandula, Geetika Sahni and Vivek Vishal Sharma for their cooperation and ever ready help.

I would like to thank Prof. Ramesh Chandra, Head of the Institute Instrumentation Centre, for providing all the instrumentation facilities during my research work.

My sincere thanks to all my family members for their moral support and encouragement to complete my project work.

I would like to express my sincere thanks to the funding source, Ministry of Human Resources and Development, Government of India, for providing me financial support during M.Tech Course of study.

Ravi Kant Sharma

RAVI KANT SHARMA

ABBREVIATIONS

Abbreviation	Full Form
RBF	Round bottom flask
$Al(ipro)_3$	Aluminium isopropoxide
Agac	Silver acetate
EtOH	Ethanol
4-NP	4-nitrophenol
4-AP	4-aminophenol
°C	Degree centigrade
g	Gram
h	Hour
mL	Milliliter
µ	Micro
nm	Nanometer
min	Minute
sec	Second

ABSTRACT

Silver-alumina nanocomposites have been synthesized by a simple thermal decomposition method using silver acetate and alumina. Two types of alumina, sol-gel alumina and commercial alumina (with / without calcination), were used as the supports in the preparation of the nanocomposites. The nanocomposites were characterized by powder X-ray diffraction (XRD), Fourier transform infrared spectroscopy (FT-IR), thermal gravimetric analysis, surface area measurements (BET), field emission scanning electron microscopy (FE-SEM) coupled with energy dispersive X-ray analysis (EDXA), transmission electron microscopy (TEM) and diffuse reflectance spectroscopy (DRS). The results indicate the presence of silver nanoparticles on the surface of alumina. It was found that the sol-gel alumina acts as a better support for the dispersion of silver nanoparticles. Also, the catalytic activity of the silver — alumina nanocomposites has been investigated by the reduction of 4-nitrophenol to 4-aminophenol using sodium borohydride.

CONTENTS

LIST OF TABLES

LIST OF FIGURES

CHAPTER 1

INTRODUCTION

CHAPTER 1
INTRODUCTION

1.1. Nanoparticles — Definition

Nanoparticles are the particles that have at least one dimension in nano range (1 to 100 nm). These particles have high surface area and surface charge density which make them highly reactive. Nanoscale materials act as a bridge between atomic and bulk matter [1].

1.2. Nanocomposites — Definition

Nanocomposite is a multi-phase solid material in which at least one phase has one of its dimensions less than 100 nanometers [2]. In general, nanocomposites exhibit better physical and chemical properties, e.g. mechanical, electrical, optical, magnetic, catalytic, etc, compared to their individual constituents [2, 3].

1.3. Types of Nanocomposites

Nanocomposites are many types and a few important ones have been discussed below.

Metal-matrix nanocomposites:

Metal-matrix nanocomposites exhibit good mechanical properties, hardness, tensile strength and ductility due to the addition of nanosized reinforcement particles into the matrix, e.g. Ni/Al_2O_3 nanocomposite [1, 4].

Polymer-matrix nanocomposites :

Polymer-matrix nanocomposites exhibit interesting physical properties due to the addition of nanoparticles to the matrix. The properties of these nanocomposites can be enhanced by better dispersion of the nanoparticles on the matrices. The properties of the nanocomposites can be affected by several factors such as extent of interphase, synthesis method, loading level of particles, size of particles, shape of particles [5], e.g. TiO_2 - polymer-matrix nanocomposites, ZnS@CdSe core-shell/poly(lauryl methacrylate) polymer matrix nanocomposite (Fig.1.1) [6], etc.

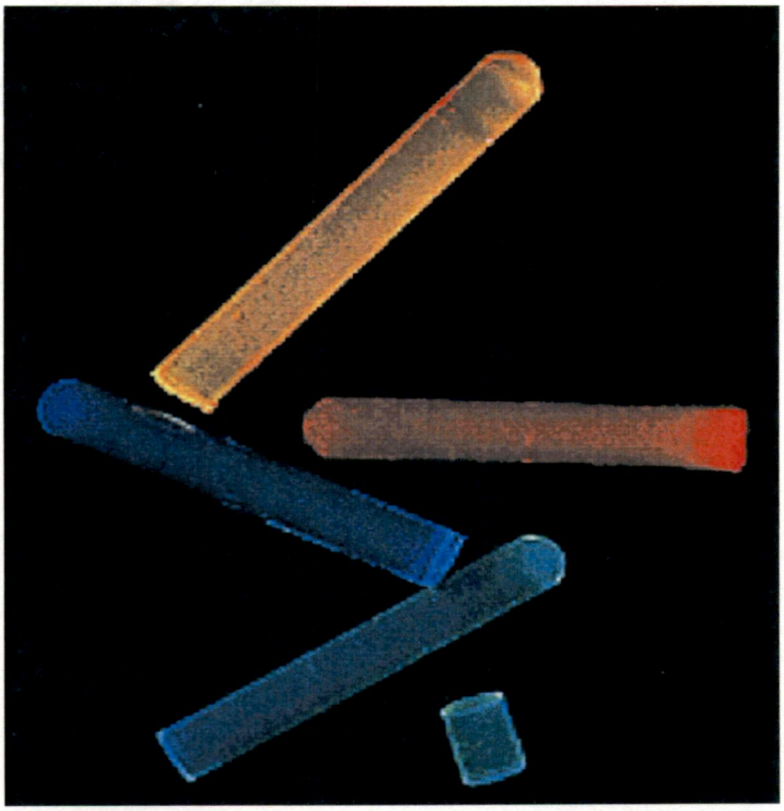

Fig.1.1. Fluorescence image of ZnS@CdSe core-shell/poly (lauryl methacrylate) polymer matrix nanocomposites.

Ceramic-matrix nanocomposites:

Ceramic-matrix nanocomposites contain finely dispersed metal nanoparticles such as Ni, Al, Cr, Mo, W, etc. incorporated into a ceramic matrix, e.g. oxide, nitride, boride, silicide.

These nanocomposites exhibit good mechanical properties. They have been widely used in applications such as heterogeneous catalysis, fuel cells, coating, microelectronics and optoelectronics [7-9]. Examples of ceramic-matrix nanocomposites include AlN/Mo, AlN/Al, Al_2O_3/Cu, MO/SiO_2, ZrO_2/Ni nanocomposites.

Metal-metal nanocomposites:

Metal-metal nanocomposites are formed by combination of two metals with different properties, e.g. Cu-Ag nanocomposites [10], Pd/Pt metal-metal nanocomposites [64] (Fig.1.2).

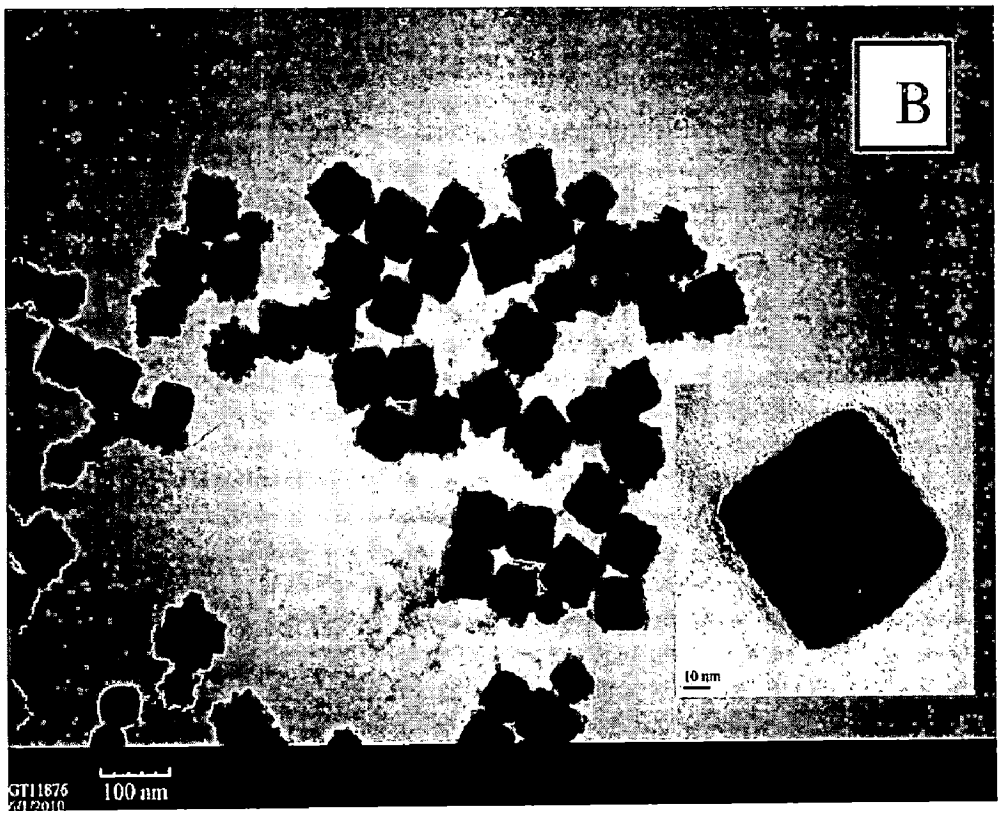

Fig.1.2. TEM image of Pd/Pt metal-metal nanocomposites [64].

1.4. Applications of Nanocomposites

Nanocomposites have been widely used because of their multi-functional properties. Nanocomposites find applications in areas such as optics [11], magnetic materials [12], sensors [13], fuels cells [14], solar cells [15], biomedical [16], catalysts [17], electronics [18], water purification [19], green chemistry [20] and ceramics [21] (Fig.1.3).

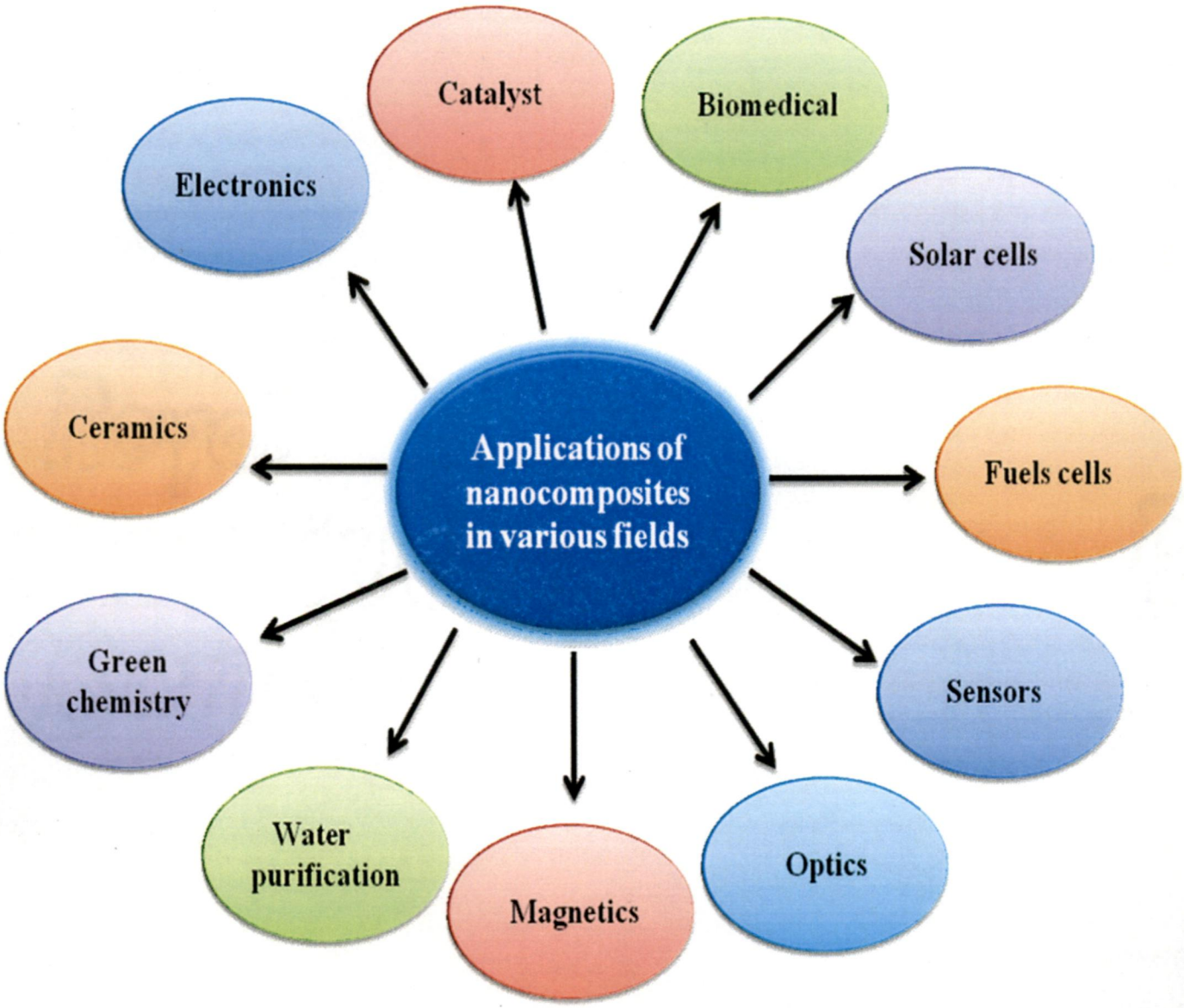

Fig.1.3. Application of nanocomposites in different fields.

- ZnO/Cu nanocomposite has been used as a good matrix in enzymatic biosensor applications [13].
- Co-CrO_3 nanocomposites exhibit interesting magnetic properties [65].
- Noble metal (Pt, Pd) — polymer nanocomposites have been used for the electrocatalytic oxidation of As (III) to As (V) [66].
- M/ZnO (M=Au, Cu, Pt) nanocomposites exhibit good optical properties [67].
- Fe_2O_3/SiO_2 nanocomposites are used in magneto optical sensors [68].
- Fe-Ni bimetallic nanocomposites have been used in the reduction of Cr (VI) to Cr (III) [69].
- TiO_2/Au (or TiO_2/Ag) has been used in dye-sensitized solar cells [70].
- Phosphotungsticacid — mesoporous silica nanocomposite has been used as an inorganic proton exchange membranes for use in direct methanol fuel cells [14].
- Magnesium-aluminate spinel — Si_3N_4 nanocomposites exhibit good mechanical properties along with optical transparency [21].
- Co-SiO_2 nanocomposites have been used as heterogeneous catalysts in oxidative degradation of chlorobenzene with H_2O_2 [71].
- Fe/Nb nanocomposite has been used in biomedical applications [72].

1.5. Silver — alumina Nanocomposites

Silver nanocomposites show good optical properties and antimicrobial activity [22] while alumina is widely being applied in different field of technologies because of its interesting and attractive properties such as easy availability, low cost, low toxicity, simple synthesis, high optical transparency, high refractive index, high melting point, hydrophobicity, favorable mechanical strength, dielectric behavior, electric insulating property and thermal and chemical stability [23-27].

Alumina is commonly used as an adsorbent, catalyst and catalyst supporting material due to its high specific surface area [28-38]. Alumina behaves as lewis acid due to the electron deficiency at the surface and has high affinity for the target anions and it can be used as absorbent for the removal of toxic metal oxyanions from water (e.g. arsenate) [39]. Electrostatic interactions occur between electron deficient sites at the surface of Al_2O_3 and the target anions during the adsorption process.

Nanocomposites based on silver-alumina nanoparticles are interesting due to their potential applications in antimicrobial activity, $DeNO_x$ activity, catalysis, optical, magnetic devices, microelectronics and sensors [27, 40-44]. For removing all types of aromatic toxic compounds, the common techniques in practice are microbial degradation, ozonation, etc. [45-47]. Recently, many authors have reported that silver nanoparticles impregnated on different type of supporting materials can be used as catalysts for the reduction of nitro aromatic compounds, especially 4-nitrophenol using $NaBH_4$ [48-53]. Silver nanoparticles act as a catalyst for electron transfer from the donor BH_4^- to the 4-nitrophenol (acceptor) [54].

The important role of Al_2O_3 is to act as the support where silver nanoparticles highly dispersed on the surface of the alumina nanoparticles show more dispersion of silver nanoparticles on their surface. The acidic nature of alumina has been considered to be the main factor to stabilize the active state of the metal species [55].

Silver — alumina nanocomposites have been synthesized by co-precipitation [55], impregnation [40], micro- emulsion [44], gel casting [56] and sonochemical methods [57]. These methods are usually expensive and take longer time for the synthesis.

In the present work, synthesis of the silver — alumina nanocomposites by a simple faster thermal decomposition method has been carried out [58].

Alumina was prepared by using minor modification of reported sol-gel method [32], The significance of the sol-gel method includes the ability of maintaining a high degree of purity, changing physical characteristics like pore size distribution, pore volume and preparing samples at low temperature with low cost and low energy consumption [33, 59]. The main factors which influence the properties of the final γ-alumina samples in the sol-gel techniques are the hydrolysis ratio (mole of water per mole of aluminum precursor), acidity of the precursor solution, etc.

CHAPTER 2

EXPERIMENTAL DETAILS

CHAPTER 2

EXPERIMENTAL DETAILS

2.1. Reagents

Aluminium isopropoxide $Al(OC_3H_7)_3$ (98%, ALDRICH®), toluene (RANKEM®), ammonia solution (25%, RANKEM®), silver acetate (SRL®), diphenyl ether (HIMEDIA®), methanol (RANKEM®), commercial alumina (RANKEM®), 4-nitrophenol (SRL®) and $NaBH_4$ (HIMEDIA®) were used as the reagents as received. Millipore water was used during the hydrolysis of aluminium isopropoxide.

2.2. Synthesis

(a) Preparation of Alumina

The flow chart for the synthesis of alumina by sol-gel method is shown in Fig.2.1. About 1.86 g of aluminium isopropoxide, 40 mL of ethyl alcohol, 25 mL of toluene and 0.5 mL of Millipore water were taken in a 100 mL round bottom flask. The contents were vigorously stirred for 3 h at room temperature till the mixture became milky white. Then, 2 mL of 25% ammonia solution was added to enhance the rate of hydrolysis. About 1 mL of Millipore water was added after 1 h and the contents was kept for constant stirring for about 24 h. The obtained slurry was evaporated at 80 °C to form a gel. Later, the gel was dried at 80 °C for overnight to obtain white powder. The powder thus obtained was calcined in air at 500 °C for 3 h inside a muffle furnace to obtain calcined alumina.

(b) Preparation of silver — alumina Nanocomposites

Silver — alumina nanocomposites were prepared by the thermal decomposition of silver acetate in diphenyl ether in the presence of alumina before and after calcination. Different nanocomposites were synthesized by varying the concentration of silver acetate (0.25, 0.5 or 1 mmol). The synthetic details are given in Table 2.1 and the procedure is given in Fig. 2.2.

About 0.041 g (0.25 mmol), 0.085 g (0.5 mmol), or 0.17 g (1 mmol) of silver acetate and 0.102 g (1 mmol) of sol-gel/commercial alumina (with/without calcination) were added to 10 mL diphenyl ether in a 50 mL round bottom flask. The contents were refluxed at 200 °C/225 °C for about 30 minutes (In the case of commercial alumina, the contents were refluxed at 225 °C). The slurries obtained were cooled to room temperature and then about 30 mL of methanol was added and the contents were centrifuged for about 20 minutes. The precipitates were washed with methanol and dried at ~ 80 °C for overnight. The powders were calcined in air at 350 °C for 3 h inside a muffle furnace. The colour of the nanocomposites before and after calcination was grey.

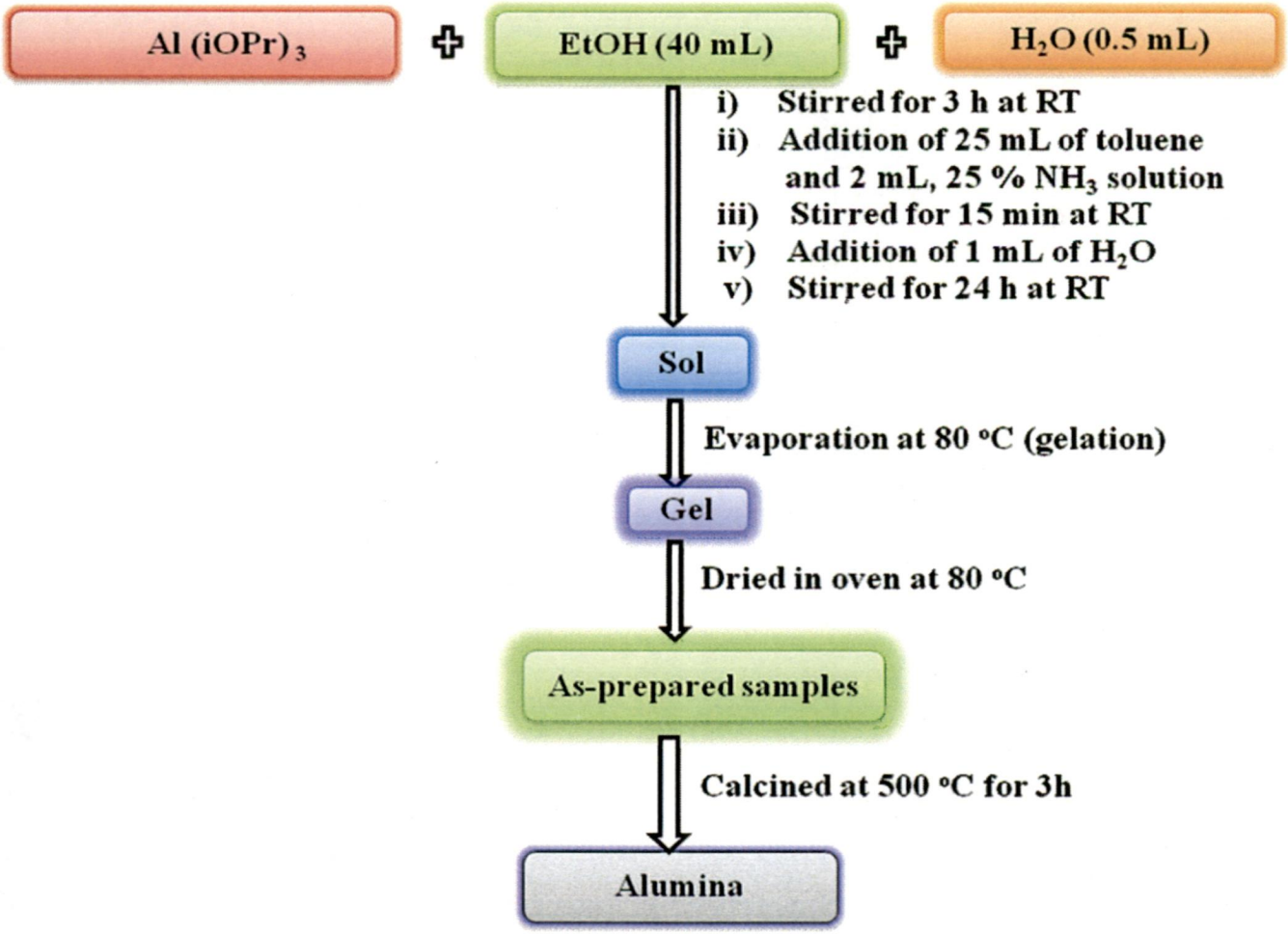

Fig.2.1. Flow chart for the synthesis of sol-gel alumina.

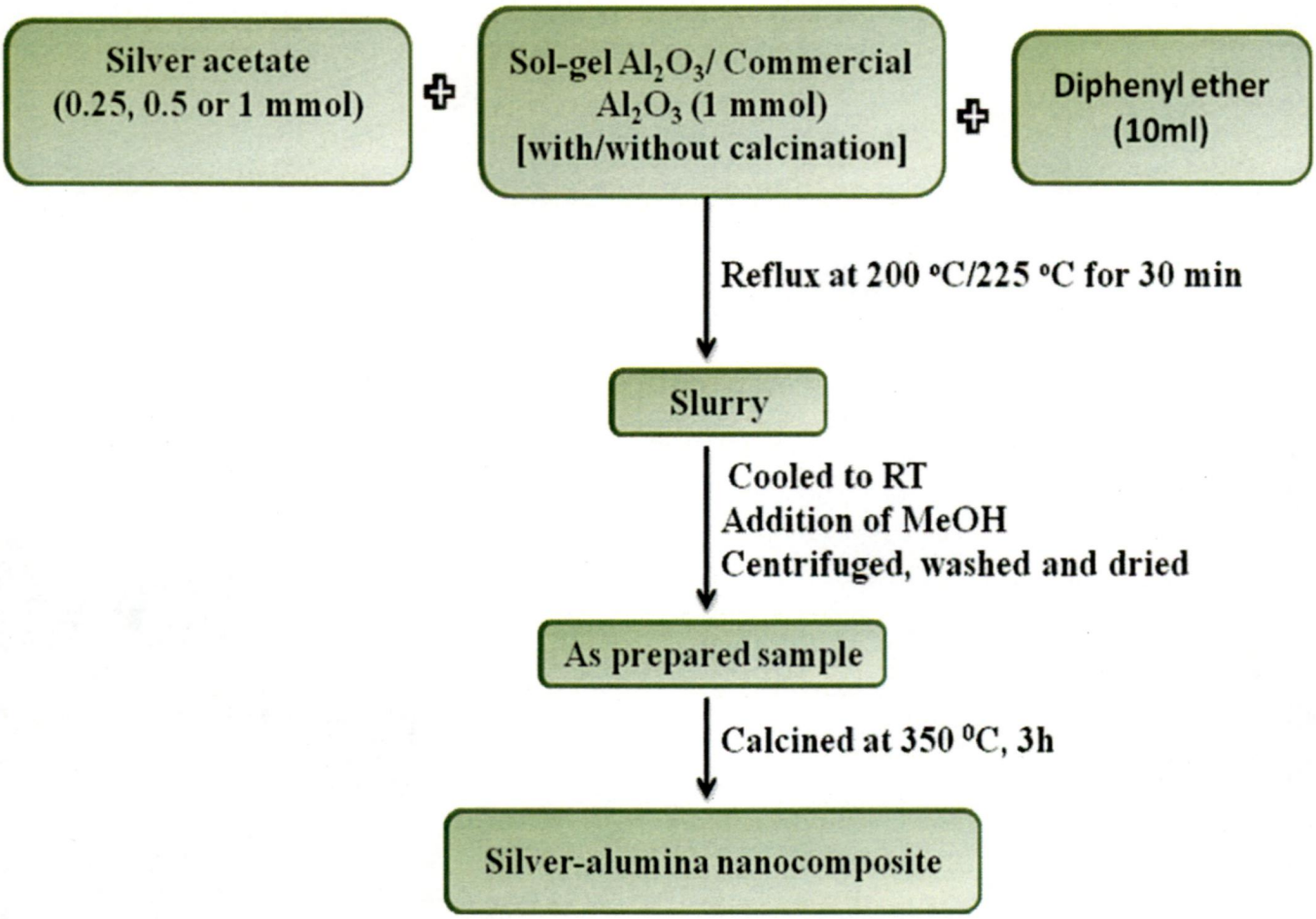

Fig.2.2. Flow chart for the synthesis of silver-alumina nanocomposites.

Table 2.1. Synthetic details of the samples prepared.

Sl. No.	Sample name	Amount of silver acetate (mmol)	Al_2O_3 type used	Colour	Yield (g)
1.	A-1	-	Sol-gel alumina without calcination	White	0.63
2.	A-2	-	Sol-gel alumina with calcination	White	-
3.	S-1	1	Sol-gel alumina with calcination	Grey	0.18
4.	S-2	1	Sol-gel alumina without calcination	Grey	0.33
5.	S-3	0.5	Sol-gel alumina with calcination	Grey	0.12
6.	S-4	0.5	Sol-gel alumina without calcination	Grey	0.12
7.	S-5	0.25	Sol-gel alumina with calcination	Grey	0.10
8.	S-6	0.25	Sol-gel alumina without calcination	Grey	0.10
9.	S-7	1	Commercial alumina with calcination	Grey	0.19
10.	S-8	1	Commercial alumina without calcination	Grey	0.13
11.	S-9	0.5	Commercial alumina with calcination	Grey	0.14
12.	S-10	0.5	Commercial alumina without calcination	Grey	0.13
13.	S-11	0.25	Commercial alumina with calcination	Grey	0.11
14.	S-12	0.25	Commercial alumina without calcination	Grey	0.11

2.3. Characterization

Pure alumina and the silver — alumina nanocomposites were characterized using powder X-ray diffraction (XRD), Fourier transform infrared spectroscopy (FT-IR), thermal gravimetric analysis, surface area measurements (BET), field emission scanning electron microscopy (FE-SEM) coupled with energy dispersive X-ray analysis (EDXA), transmission electron microscopy (TEM) and diffuse reflectance spectroscopy (DRS).

Powder XRD patterns were recorded on a Brucker AXS D8 diffractometer operating with Cu-Kα radiation (λ=1.5406 Å) with a scanning speed of 2°/min. A Thermo Nicolet Nexus Fourier FT-IR spectrophotometer was used for recording the IR spectra using KBr pellets. Thermal gravimetric measurements were carried out using a Perkin Elmer (Pyris Diamond) instrument in nitrogen atmosphere at a heating rate of 5°/min. The specific surface area of the samples were measured from the nitrogen adsorption data using the Brunauer-Emmett-Teller (BET) technique by Micromeritics chemisorb 2720 instrument. The morphology of the samples along with elemental analysis (EDXA) data were obtained using a FEI Quanta 200F microscope operating at 20 KV. TEM images of the samples were recorded on a FEI TECNAI G2 electron microscope operating at an accelerating voltage of 200 KV. Carbon coated copper grids were used for the TEM studies. UV-visible reflectance spectra were recorded on a Shimadzu UV-2450 UV-Visible-NIR spectrophotometer using a diffuse reflectance accessory in the wavelength region 200 to 600 nm using barium sulphate as the reference.

2.4. Catalytic Activity Test

The catalytic activity of the silver — alumina nanocomposites was investigated by the reduction of 4-nitrophenol to 4-aminophenol using $NaBH_4$ as the reducing agent [44]. To about 50 mL aqueous solution of 4-nitrophenol (0.1 mmol), 50 mL of freshly prepared aqueous solution of $NaBH_4$ (0.529 mol/L) was added. Then about 20 mg of the catalyst (silver — alumina nanocomposites) was added to the reaction mixture and the contents were kept for constant stirring at room temperature. The complete reduction of 4-nitrophenol (yellow coloured solution) was indicated by the decolorization of the solution.

CHAPTER 3

RESULTS AND DISCUSSION

CHAPTER 3
RESULTS AND DISCUSSION

3.1. XRD Analysis

The XRD pattern of the sol-gel alumina before calcination (Fig.3.1) show peaks due to boehmite (JCPDS file no. 01-0774). After calcination at 500 °C, peaks due to γ-Al_2O_3 (JCPDS file no. 29-0063) are observed. The XRD pattern of the silver — sol-gel alumina nanocomposite samples before calcination (Fig.3.2) show peaks only due to silver (JCPDS file no. 03-0921). After calcination at 350 °C the nanocomposite samples (Fig.3.3) show weak reflections ($2\theta \approx 19.3^{\circ}$ and 33.8°) due to $AgAlO_2$ (JCPDS file no. 21-1070).

The crystallite size for the silver present in the calcined silver — sol-gel alumina nanocomposites was calculated using Debye-Scherrer's formula as given below [60].

$$\delta = 0.89\,\lambda / \beta \cos\theta$$

Where δ is the crystallite size in nm. 0.89 represents a dimensionless constant k, λ is the wavelength of Cu-Kα (1.5406 Å), β is full width at half maxima and θ is the angle. The calculated crystallite size values of silver in the nanocomposites are given in Table 3.1. The crystallite size of silver varies from 13.0 to 38.9 nm. The lowest crystallite size was obtained for the sample S-2, and the highest crystallite size was obtained for the sample S-1.

The XRD patterns of silver — commercial alumina nanocomposites before and after calcination (Figs.3.4 and 3.5) show peaks due to silver (JCPDS file no. 03-0921) and a small peak due to γ-Al_2O_3 (JCPDS file no. 29-0063). The crystallite size for the silver present in the calcined silver — commercial alumina nanocomposites varies from 15.5 to 39.9 nm. The lowest crystallite size was obtained for the sample S-12 and highest crystallite size was obtained for the sample S-7.

The crystallite size of Ag nanoparticles supported on sol-gel alumina is in general smaller when compared to that on commercial alumina.

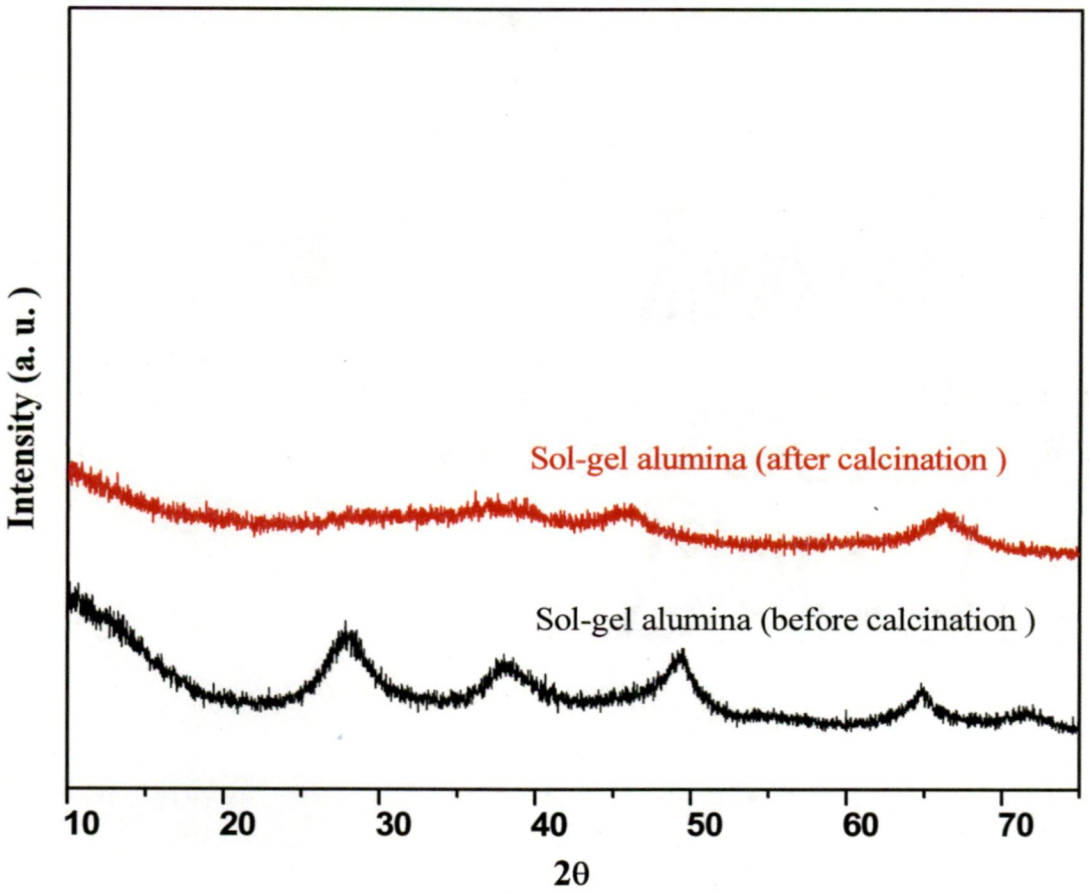

Fig.3.1. XRD patterns for the sol-gel alumina before and after calcination.

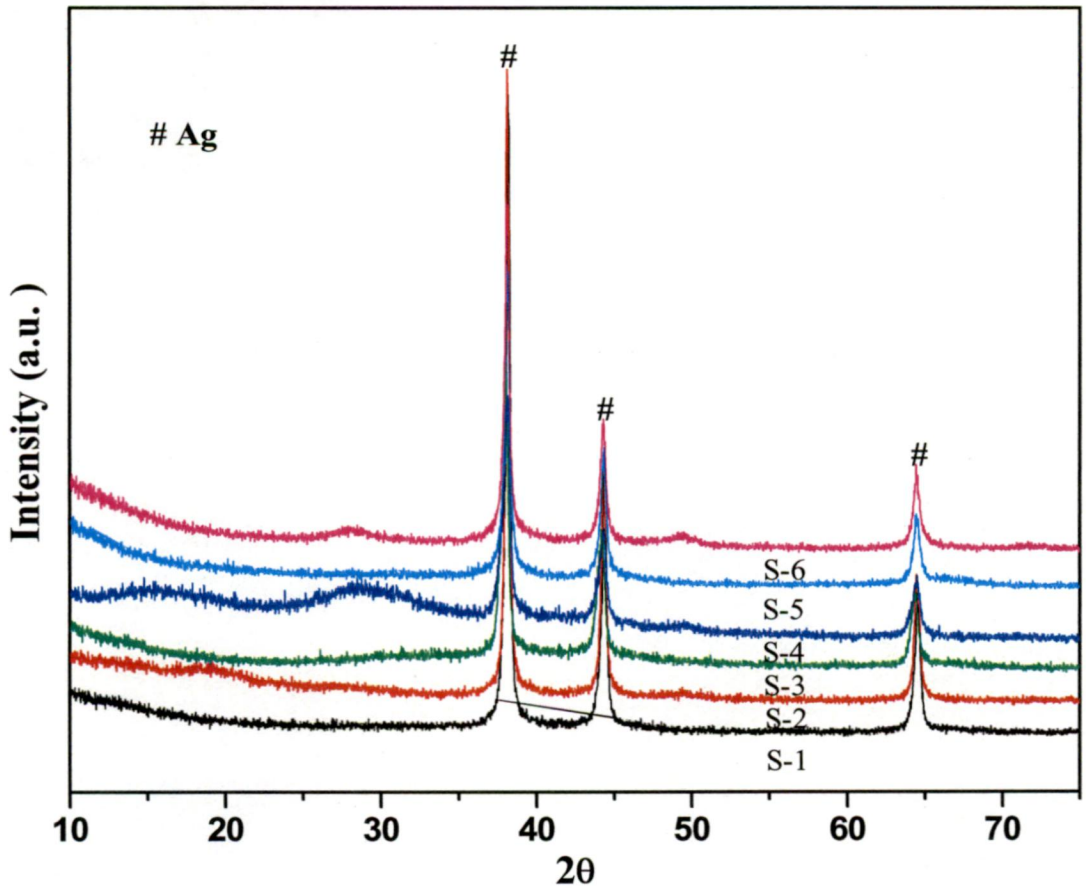

Fig.3.2. XRD patterns for the silver – sol-gel alumina nanocomposites before calcination. The synthetic details of the nanocomposites are given in Table 1.

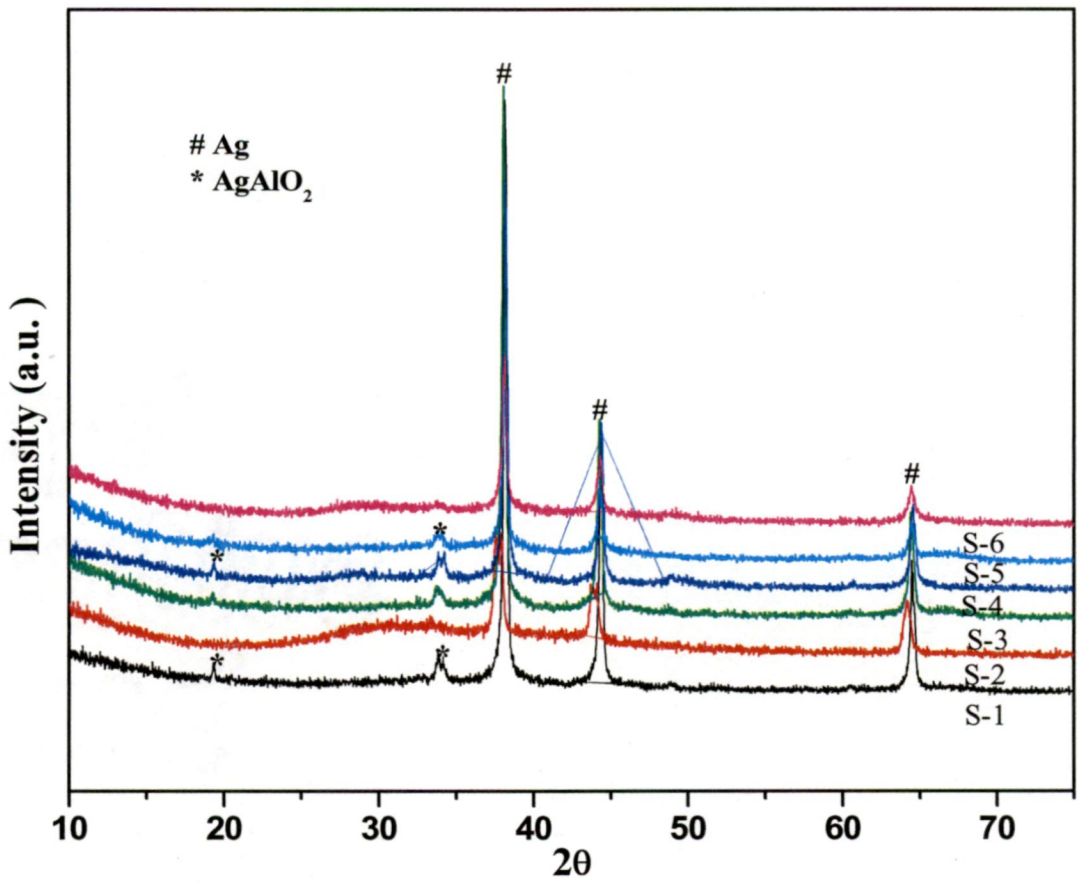

Fig.3.3. XRD patterns for the silver – sol-gel alumina nanocomposites after calcination.

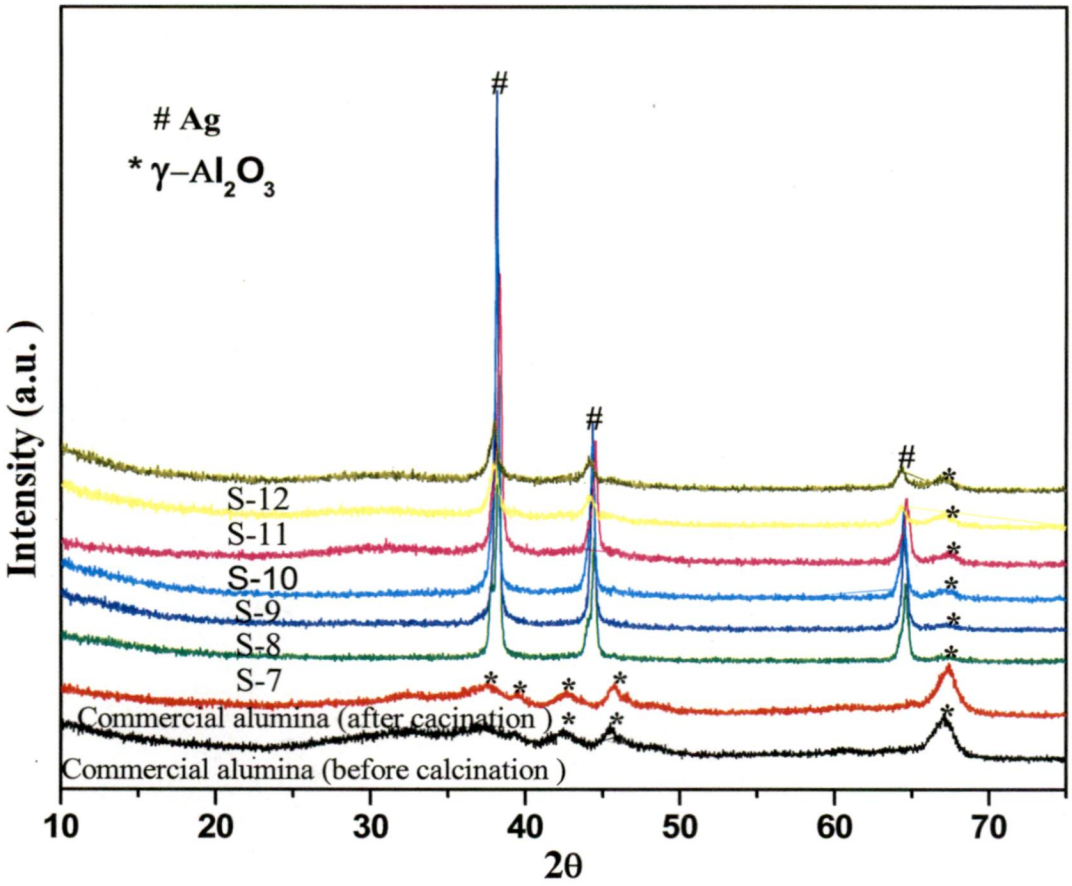

Fig.3.4. XRD patterns for the silver – commercial alumina nanocomposites before calcination.

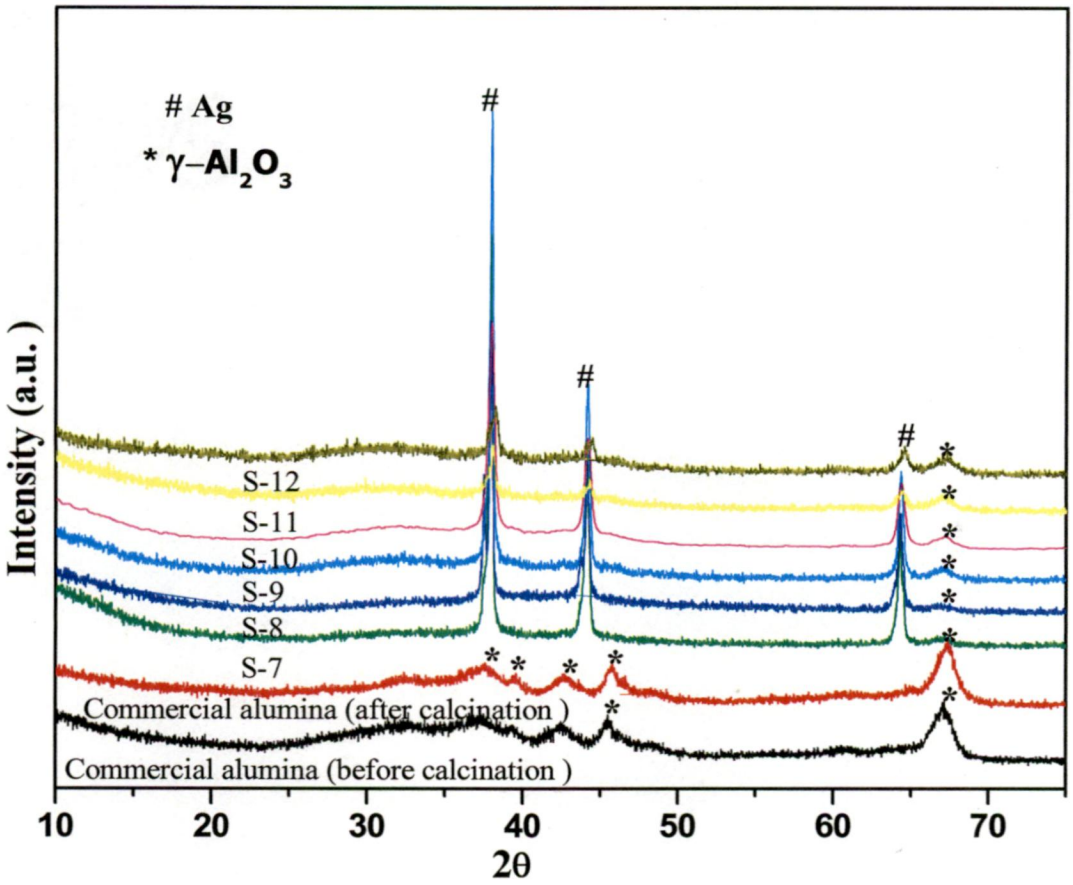

Fig.3.5. XRD patterns for the silver – commercial alumina nanocomposites after calcination.

Table 3.1. Crystallite size (nm) of silver present in the nanocomposites before and after calcination.

Sl. No.	Sample ID	Crystallite size of Ag in the nanocomposites (nm)	
		Before calcination	After calcination
1.	S-1	28.0	38.9
2.	S-2	24.9	13.0
3.	S-3	23.8	30.0
4.	S-4	21.4	32.9
5.	S-5	20.8	25.8
6.	S-6	24.9	30.8
7.	S-7	32.4	39.9
8.	S-8	35.6	36.1
9.	S-9	33.4	36.2
10.	S-10	29.0	33.4
11.	S-11	14.4	27.6
12.	S-12	16.3	15.5

3.2. FT-IR Analysis

The IR spectra of the alumina prepared by sol-gel method (before and after calcination) are shown in Fig. 3.6. The band positions and their assignments are given Table 3.2 [28, 32, 61]. The bands near 3500 cm^{-1} are due to the O-H stretching which arise from adsorbed moisture and the present in the KBr used for making the pellets. The weak bands at about 2930 and 2858 cm^{-1} can be assigned to the stretching vibrations of C-H [28]. The bands around 1644 cm^{-1} in both the as-prepared and the calcined samples are due to the bending vibration of water molecules [36]. The IR spectra of silver — sol-gel alumina nanocomposites before and after calcination (S-1 to S-6) are shown in Figs.3.7 and 3.8. The band positions and their assignments are given Table 3.3 and 3.4 [28, 32, 36]. The bands observed between 1585 and 1387 cm^{-1} in the nanocomposites before calcination are attributed to the presence of (C=O), carbon-carbon (C-C) and carbon-hydrogen (CH_3) deformation mode and the bands almost disappear after calcination [28, 32]. The bands at about 1168 cm^{-1} and 1070 cm^{-1} in the case of nanocomposites before calcination are attributed to the ν_{asym}.Al-O-H and ν_{sym}.Al-O-H modes of boehmite, respectively. These bands almost disappear in the calcined samples [28]. The band near 884 cm^{-1} is attributed to the Al-O band in the nanocomposites before calcination [61]. The bands near 639 and 480 cm^{-1} can be attributed to the bending modes of AlO_6 units in alumina nanoparticles while the bands near 752 and 783 cm^{-1} are attributed to the bending vibration of AlO_4 [32].

The IR spectra of silver — commercial alumina nanocomposites before and after calcination (S-7 to S-12) are shown in Figs.3.9 and 3.10. The band positions and their assignments are given in Tables 3.5 and 3.6.

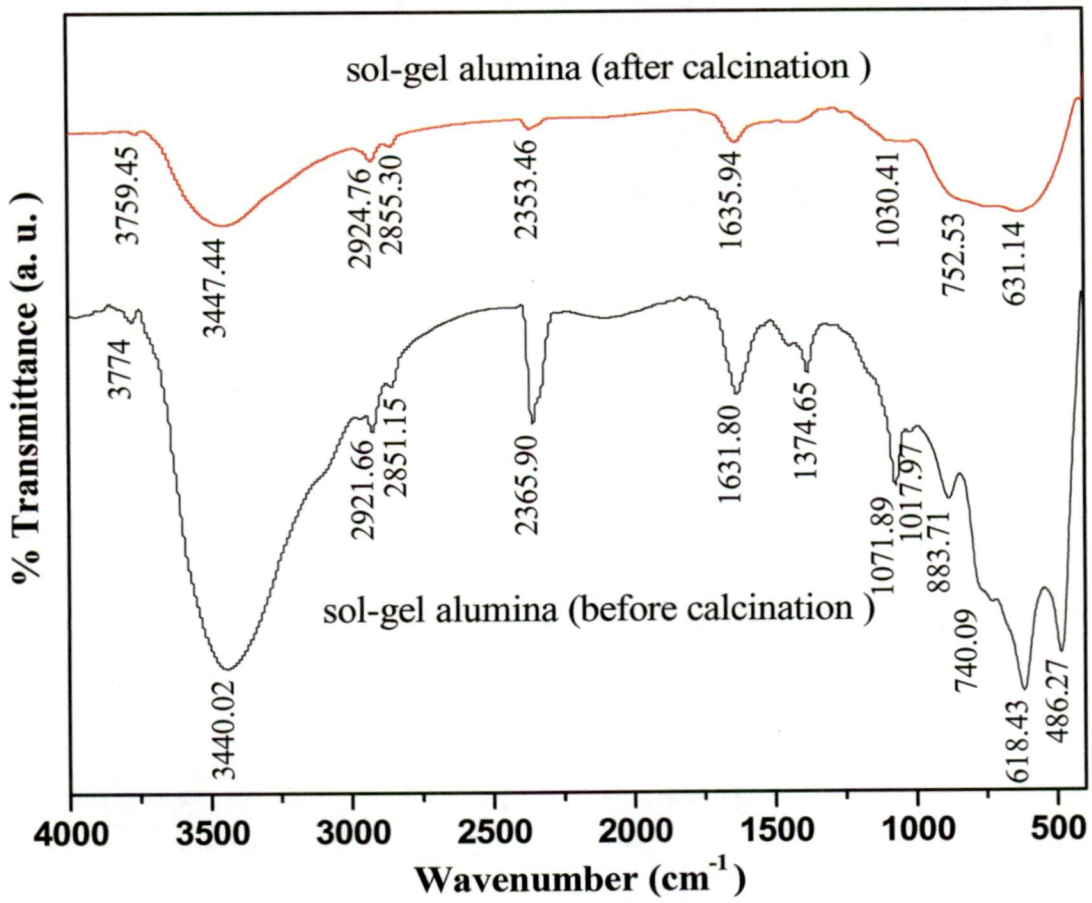

Fig.3.6. FT-IR spectra for the sol-gel alumina before and after calcination.

Table 3.2. FT-IR band positions and assignments of the sol-gel alumina before and after calcination.

Observed band position (cm^{-1}) for sol-gel Al_2O_3		**Assignment of bands**
Before calcination	**After calcination**	
3440	3447	O-H str.
1631	1635	O-H bending
1374	-	C-O str.
1071	-	Asymmetric (Al-O-H) str.
1017	1030	Sym. (Al-O-H) str.
884	-	Al-O str.
740	752	Bending vibration of AlO_4
618	631	Bending vibration of AlO_6

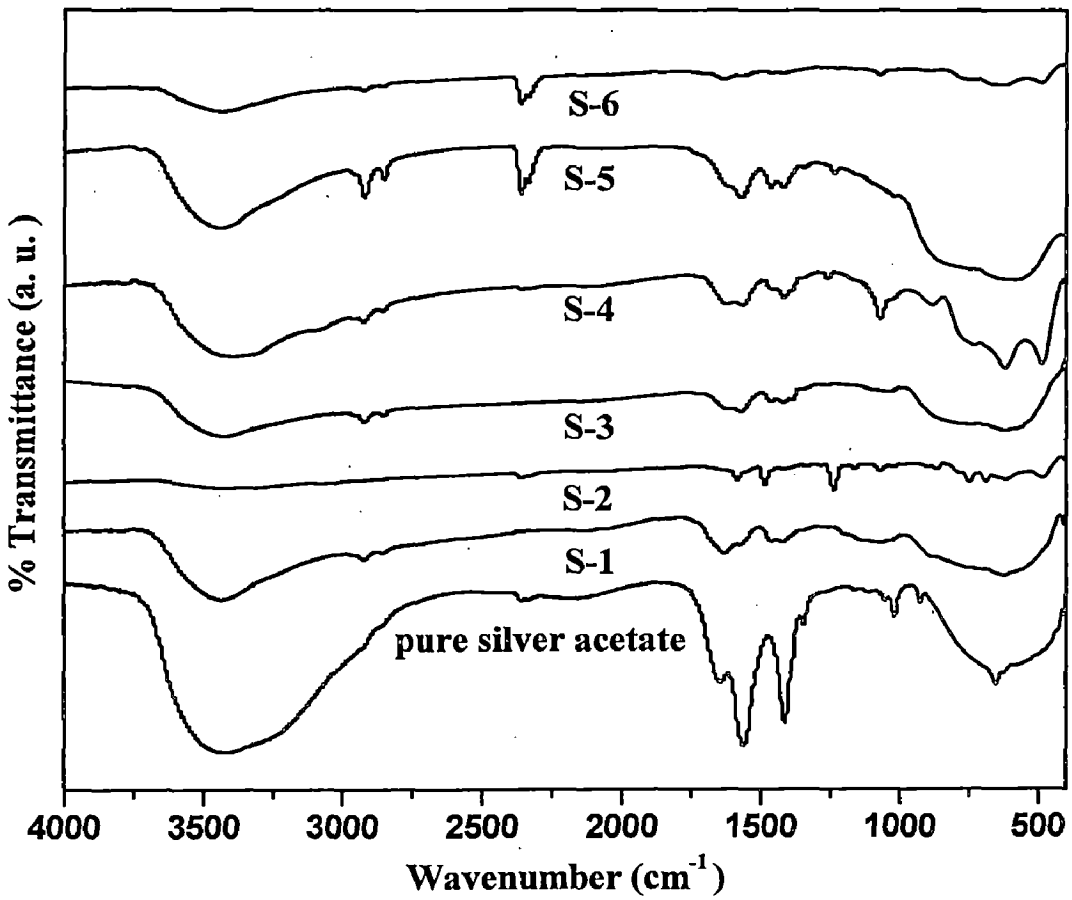

Fig.3.7. FT-IR spectra for the silver — sol-gel alumina nanocomposites before calcination.

Table 3.3. FT-IR band positions and their assignments of the silver — sol-gel alumina nanocomposites before calcination.

Observed band position (cm^{-1})							Assignment of the bands
Silver acetate	**S-1**	**S-2**	**S-3**	**S-4**	**S-5**	**S-6**	
3413	3432	3419	3427	3392	3447	3438	(O-H) str.
-	2923 2851	2913 2847	2923 2859	2921 2855	2926 2851	2923 2859	Sym.(C-H) str.
1643	1629	1609	1627	1623	-	1644	O-H bending
1570	1565	1585	1572	1560	1569	1572	Asym. C=O str.
1411	1453, 1416	1484, 1411	1465, 1415	1457, 1413	1469, 1422	1460, 1419	Asym. (CH_3) deformation
1341	-	1329	1382	-	1348	-	Sym. (CH_3) deformation
1167, 1121	1145	1163	1104	1168	-	1162	$\nu_{asym.}$(O-H) in alcohol, water and Al-O-H
1055	1059	1070	1031	1069	1023	1073	ν_{sym}.(O-H) in alcohol, water and Al-O-H
922	-	901	-	-	-	-	(C-C) str.
-	881	864	-	881	-	888	Al-O str.
652	-	-	-	-	-	-	(O-C-O) rocking
-	723	749, 690	748	727	750	751	Bending vibration of AlO_4
-	625	618	624	619	601	639	Bending vibration of AlO_6

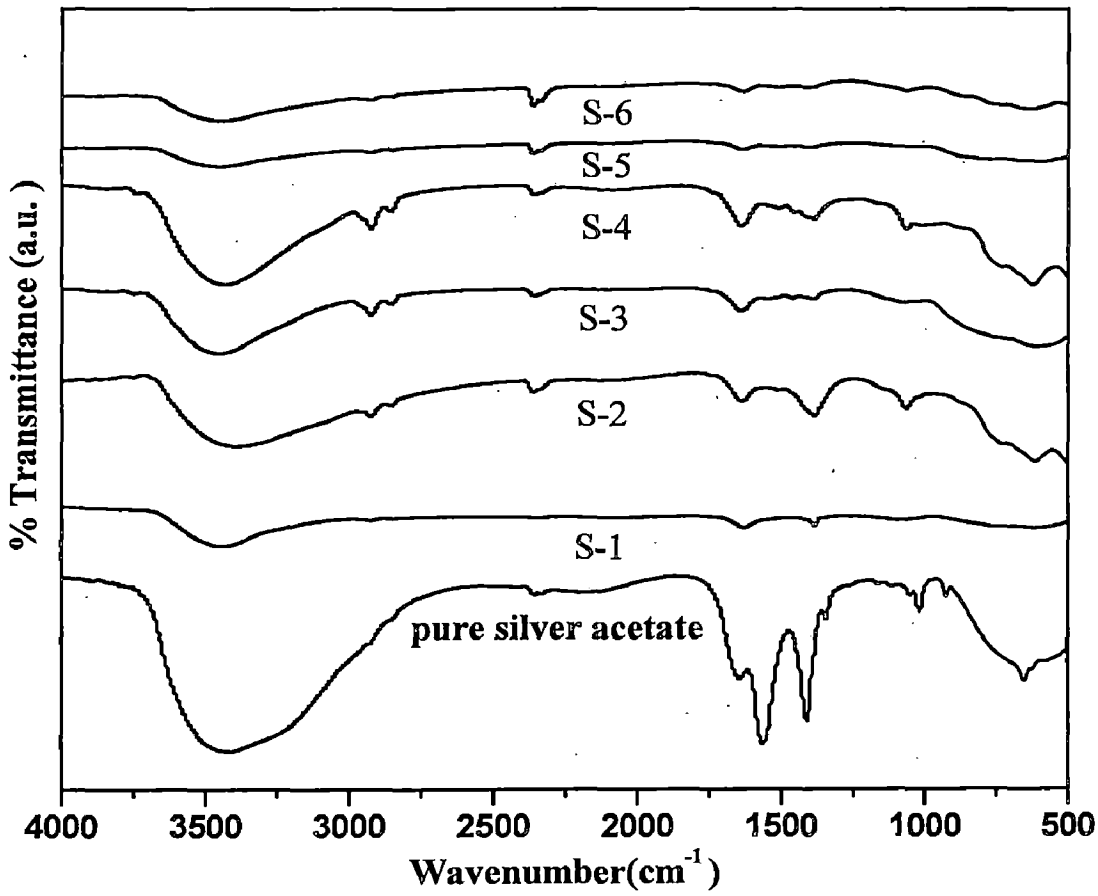

Fig.3.8. FT-IR spectra for the silver — sol-gel alumina nanocomposites after calcination.

Table 3.4. FT-IR band positions and their assignments for the silver — sol-gel alumina nanocomposites after calcination.

Observed band position (cm^{-1})							Assignment of the bands
Silver acetate	**S-1**	**S-2**	**S-3**	**S-4**	**S-5**	**S-6**	
3413	3438	3394	3448	3444	3452	3454	(O-H) str.
-	2925	2925, 2847	2929, 2851	2925, 2855	2923, 2859	2931, 2859	Sym.(C-H) str.
1643	1630	1644	1644	1635	1636	1636	O-H bending
1570	-	-	-	-	1512	1508	Asym. C=O str.
1411	-	-	1461	-	1419	1411	Asym. (CH_3) deformation
1341	1384	1378	1382	1387	-	-	Sym. (CH_3) deformation
1167, 1121	-	-	-	-	1140	-	ν_{asym}.(O-H) in alcohol, water and Al-O-H
1055	1096	1067	1076	1059	-	1065	ν_{sym}.(O-H) in alcohol, water and Al-O-H
922	-	-	-	-	-	-	(C-C) str.
-	-	882	-	880	884	874	Al-O str.
652	-	-	-	-	-	-	(O-C-O) rocking
-	752	731	752	740	782	744	Bending vibration of AlO_4
-	618	613	612	629	599	639	Bending vibration of AlO_6

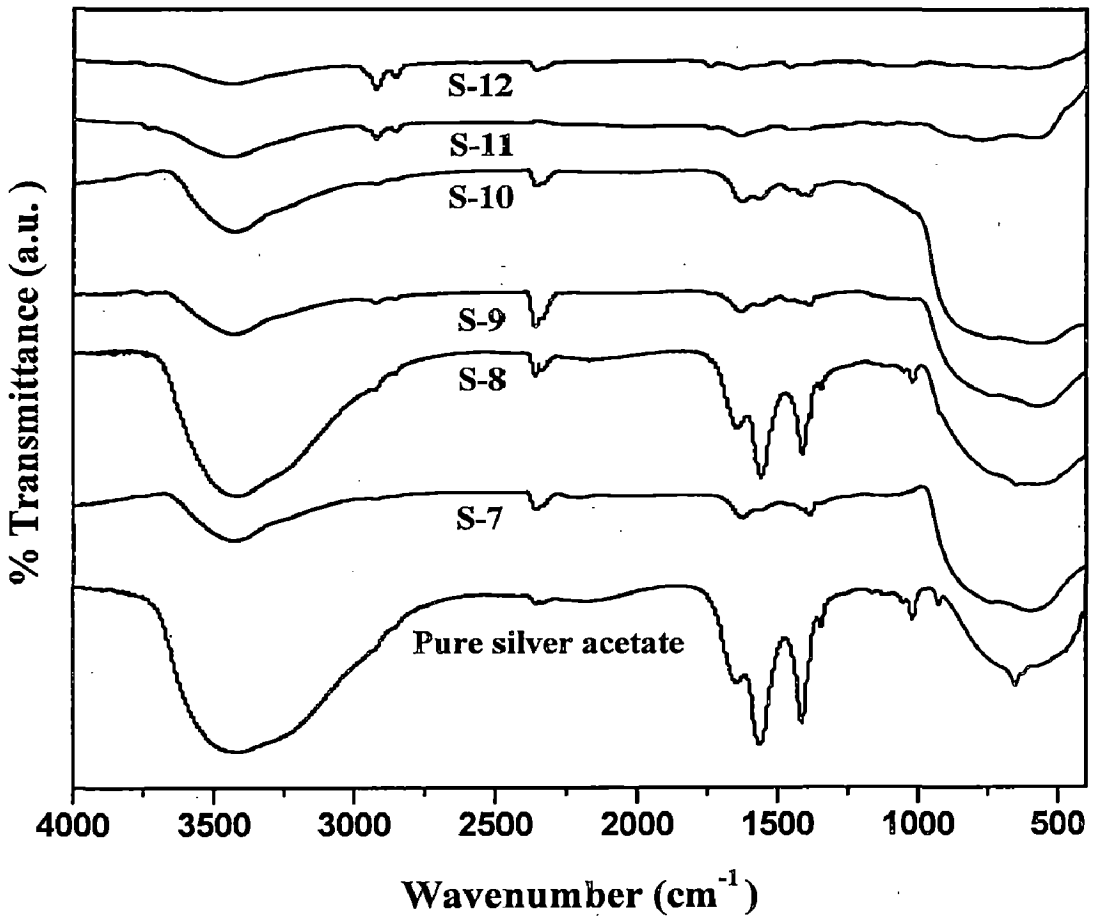

Fig.3.9. FT-IR spectra for the silver — commercial alumina nanocomposites before calcination.

Table 3.5. FT-IR band positions and their assignments for the silver — commercial alumina nanocomposites before calcination.

Observed band position (cm^{-1})							Assignment of the bands
Silver acetate	**S-7**	**S-8**	**S-9**	**S-10**	**S-11**	**S-12**	
3413	3430	3430	3433	3420	3455	3455	(O-H) str.
-	2930	2916 2855	2922 2855	2919 2858	2926 2861	2918 2851	Sym.(C-H) str.
1643	1625	1638	1628	1624	1635	1635	O-H bending
1570	1559	1516	1552	1556	-	-	Asym. C=O str.
1411	1410	1417	1450	1459	1461	1463	Asym.(CH_3) deformation
1341	1378	1338	1381	1397	1378	1378	Sym.(CH_3) deformation
1167, 1121	1151	1132	1104	-	1163, 1122	1163, 1122	$\nu_{asym.}$(O-H) in alcohol, water and Al-O-H
1055	-	1055	1021	-	1034	1038	ν_{sym}.(O-H) in alcohol, water and Al-O-H
-	-	-	-	-	884	-	(C-C) str.
922	-	-	-	-	-	-	Al-O str.
652	-	655	-	-	-	-	(O-C-O) rocking
-	740	738	734	756	783	738	Bending vibration of AlO_4
-	594	540	580	588	584	615, 576	Bending vibration of AlO_6

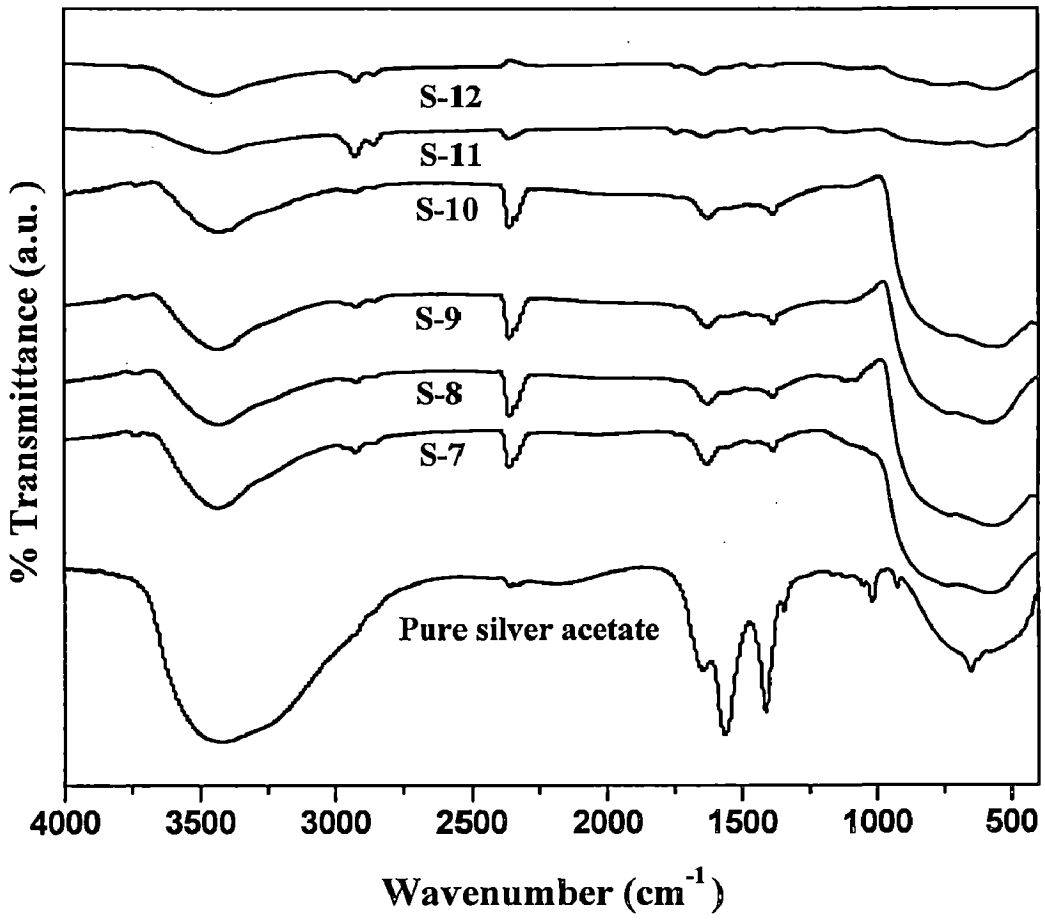

Fig. 3.10. FT-IR spectra for the silver — commercial alumina nanocomposites after calcination.

Table 3.6. FT-IR band positions and their assignments of the silver — commercial alumina nanocomposites after calcination.

Observed band position (cm^{-1})							Assignment of the bands
Silver acetate	**S-7**	**S-8**	**S-9**	**S-10**	**S-11**	**S-12**	
3413	3432	3434	3434	3432	3447	3438	(O-H) str.
-	2922 2853	2917 2846	2919 2847	2920 2852	2934 2851	2918 2851	Sym.(C-H) str.
1643	1627	1624	1628	1626	1636	1635	O-H bending
1570	1550	1553	1565	-	1569	-	Asym. (C=O) str.
1411	1457	1463	1456	-	1453	1461	Asym. (CH_3) deformation
1341	1380	1383	1386	1380	1378	1378	Sym. (CH_3) deformation
1167, 1121	-	1127	1116	1105	1172, 1106	1114	$\nu_{asym.}$(O-H) in alcohol, water and Al-O-H
1055	-	1071	-	1096	-	1031	ν_{sym}.(O-H) in alcohol, water and Al-O-H
922	-	-	-	-	-	-	(C-C) str.
-	-	-	-	-	890	890	Al-O str.
652	-	-	-	-	-	-	(O-C-O) rocking
-	741	724	726	727	733	763	Bending vibration of AlO_4
-	581	590	580	556	584, 522	570	Bending vibration of AlO_6

3.3. Thermal Gravimetric Analysis

Thermal gravimetric analysis of the as prepared nanocomposites prepared using sol-gel alumina and commercial alumina (with/without calcination) have been carried out in the temperature range 27 °C to 1000 °C with a heating rate of 5 °C min^{-1}. The typical thermograms of the nanocomposites are shown in Figs.3.11 and 3.12. The percentage weight losses for the samples are given in Table 3.7. TGA results show weight loss up to 500 °C for all the nanocomposites. Sol-gel alumina shows more weight loss (34.7%) compared to commercial alumina (7.3%). Silver — sol-gel alumina nanocomposites also show more weight loss (8.6 to 24.0%) compared to silver — commercial alumina nanocomposites (3.2 to 9.6%). The weight loss below 150 °C is attributed to the physically adsorbed water and other gas molecules. The weight loss in the region 150-500 °C is due to the dehydration of AlOOH to Al_2O_3 and also the removal of organic species [28, 32]. There is nearly no weight loss at temperatures above 500 °C.

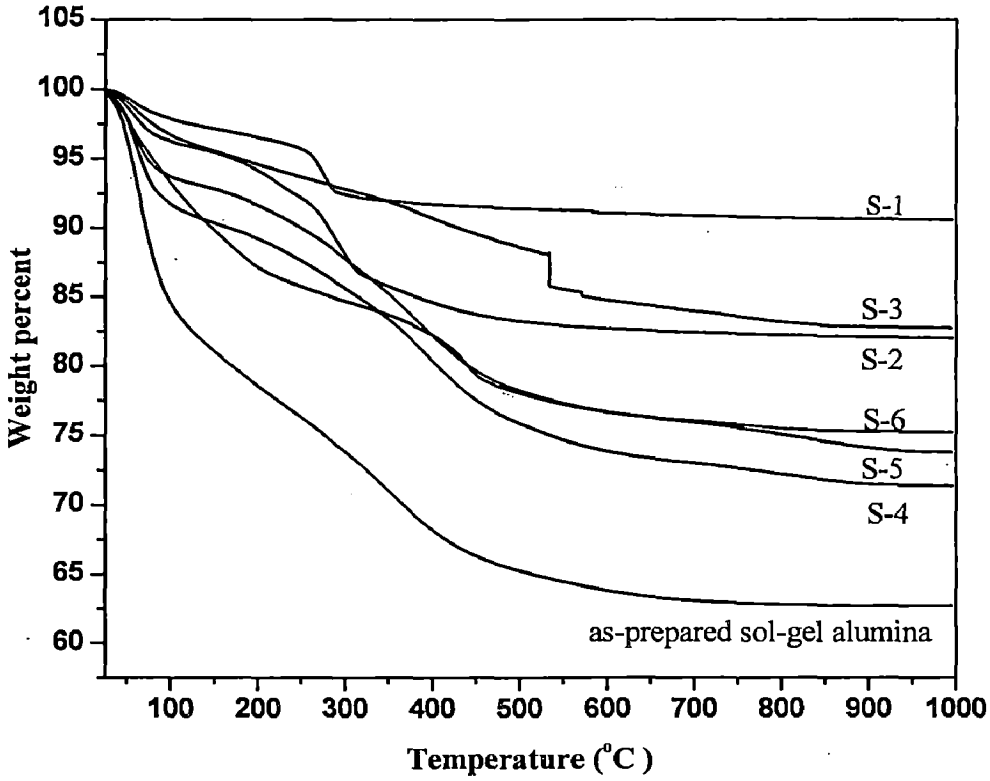

Fig.3.11. TGA curves of the silver — sol-gel alumina nanocomposites before calcination.

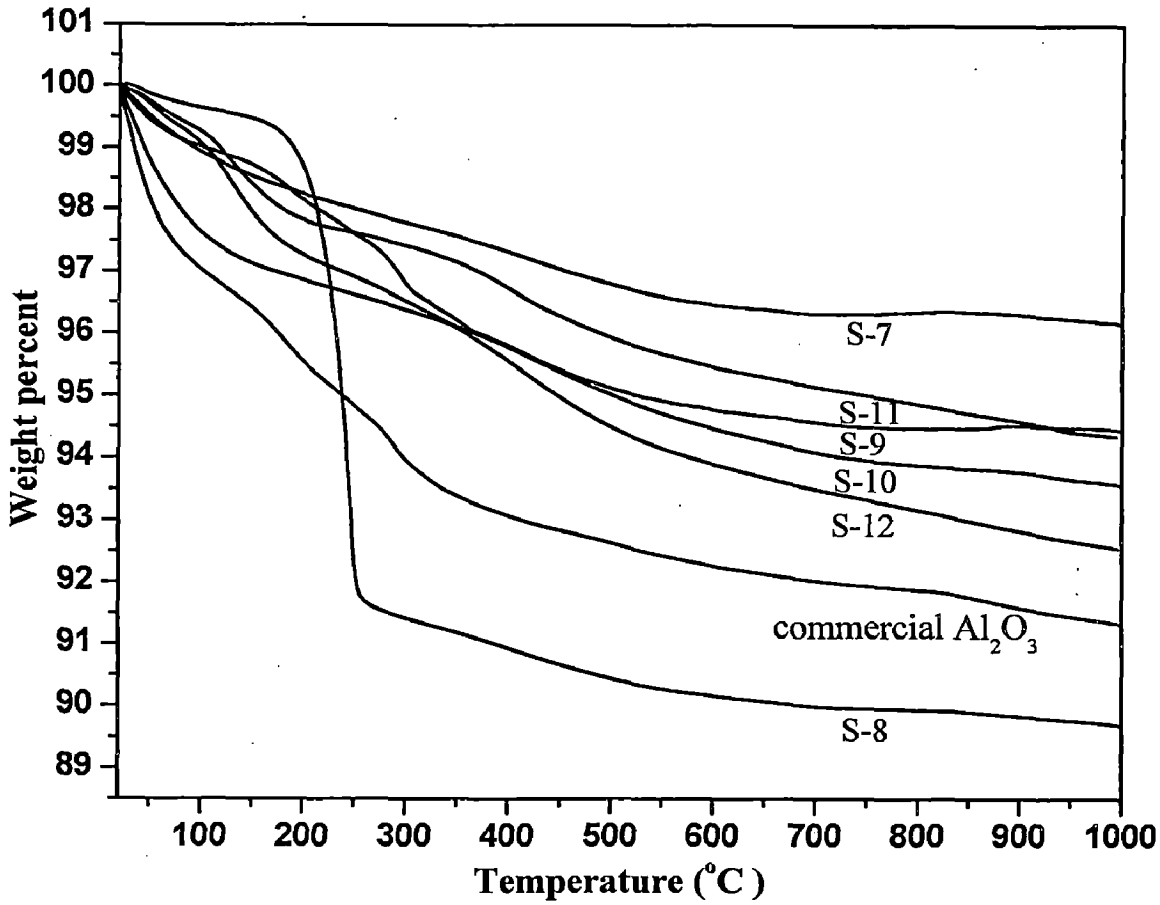

Fig.3.12. TGA curves of the silver — commercial alumina nanocomposites before calcination.

Table 3.7. Percentage weight losses for the sol-gel alumina, commercial alumina and the silver — alumina nanocomposites.

Sample	% Wt. loss (Up to 500°C)
Sol-gel alumina	34.73
S-1	8.59
S-2	16.73
S-3	12.98
S-4	21.74
S-5	21.95
S-6	24.07
Commercial alumina	7.3
S-7	3.2
S-8	9.6
S-9	4.9
S-10	5
S-11	4.05
S-12	5.49

3.4. Surface Area Analysis (BET)

Surface area measurements (BET) were carried out on sol-gel alumina, commercial alumina, silver — alumina (sol-gel/commercial) nanocomposites (S-6, S-12). The specific surface area values and the total pore volume are given in Table 3.8. The results indicate that the sol-gel alumina has a very high specific surface area (525.65 $m^2 g^{-1}$) and total pore volume (0.2646 $cm^3 g^{-1}$) compared to that of commercial alumina (surface area ~ 101.89 $m^2 g^{-1}$) and total pore volume (0.0513 $cm^3 g^{-1}$). Also, the silver — sol-gel alumina nanocomposite (S-6) has high specific surface area and total pore volume compared to that of silver — commercial alumina nanocomposite (S-12).

Table 3.8. BET surface area and total pore volume of pure alumina and silver — alumina nanocomposites.

Sample	BET surface area ($m^2 g^{-1}$)	Total pore volume ($cm^3 g^{-1}$)
Sol-gel alumina	525.65	0.2646
Commercial alumina	101.89	0.0513
S-6	267.41	0.1346
S-12	60.31	0.0304

3.5. FE-SEM / EDX Analysis

The SEM images of the sol-gel or commercial alumina (before and after calcination) and Ag — alumina nanocomposites (before and after calcination) are shown in Figs. 3.13-3.17. The SEM images of the sol-gel alumina (before and after calcination) and commercial alumina show the presence of agglomerated particles with close to spherical morphology.

The SEM images of the silver — sol-gel alumina nanocomposites before calcination show agglomeration of particles. After calcination, the agglomeration of particles is increased and the particles exhibit close to spherical morphology.

The SEM images of the silver — commercial alumina nanocomposites consist of agglomeration of larger particles and with close to spherical morphology and irregular size.

EDX analysis results indicate the presence of carbon, oxygen, aluminium and silver in all the nanocomposites. The weight % of various elements present in the nanocomposites are given in Table 3.9. The weight % of Ag varies from about 4.4 to 48.4 % for silver — sol-gel alumina nanocomposites and the weight % of Ag varies from 16.5 to 84.0 % in silver — commercial alumina nanocomposites. When sol-gel alumina before or after calcination is employed during the thermal decomposition of silver acetate in diphenyl ether, with the increase in concentration of the silver acetate (0.25 to 1 mmol), the silver weight % is increasing. When commercial alumina after calcination is employed during the thermal decomposition of silver acetate, with increase in the concentration of silver acetate (0.25 to 1 mmol), the silver weight percent is increasing in the nanocomposites. On the other hand, the amount of silver remains the same in the case of nanocomposites prepared using commercial alumina without heat treatment (i.e. before calcination).

The EDXA data indicate almost uniform distribution of silver in silver — sol-gel alumina nanocomposites compared to that in silver — commercial alumina nanocomposites.

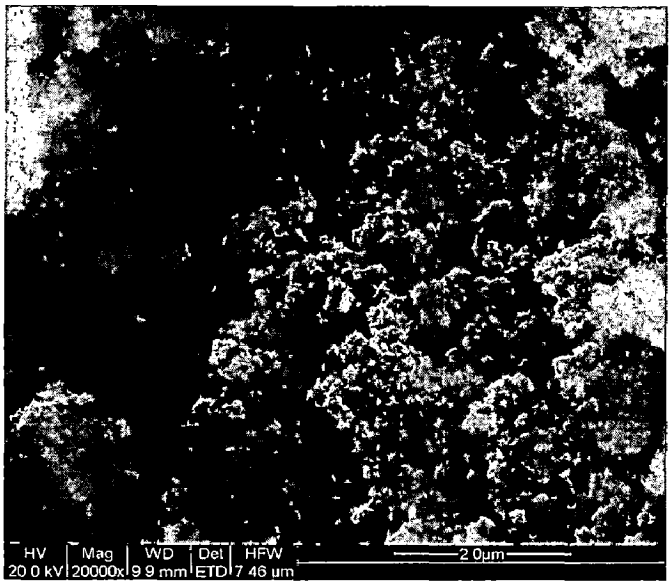

Sol-gel alumina (before calcination)

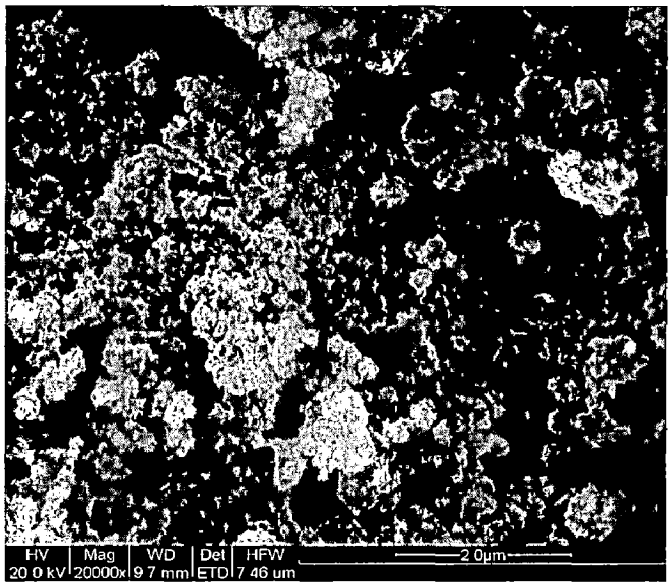

Sol-gel alumina (after calcination)

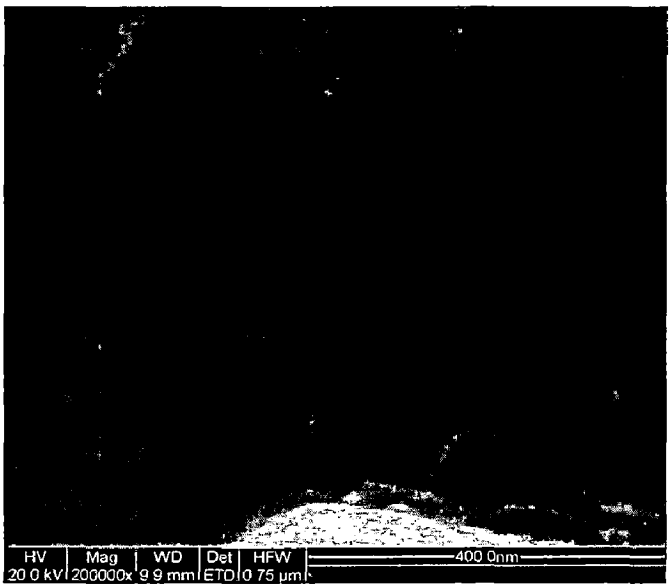

Commercial alumina

Fig.3.13. FE-SEM images of sol-gel alumina (before and after calcination) and commercial alumina.

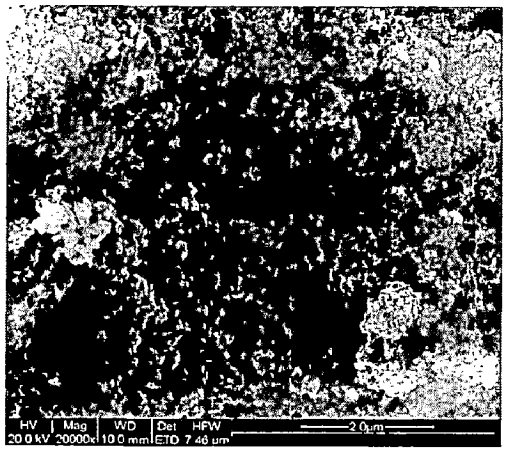

S-1

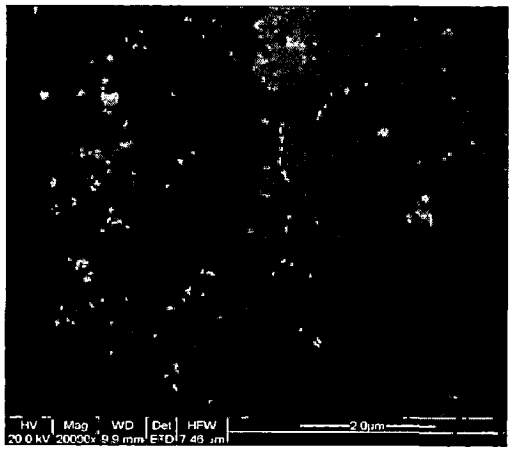

S-2

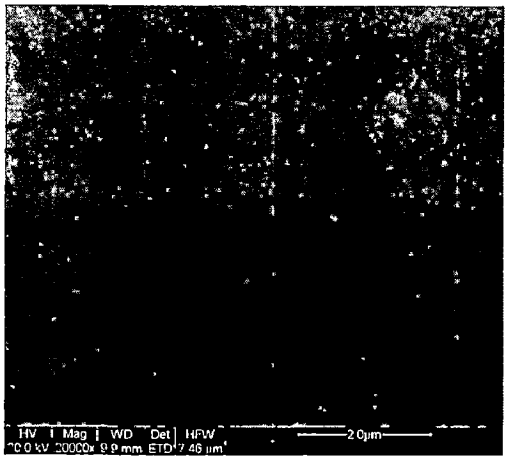

S-3

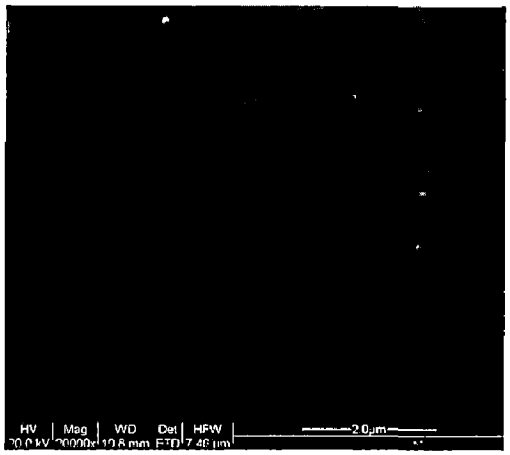

S-4

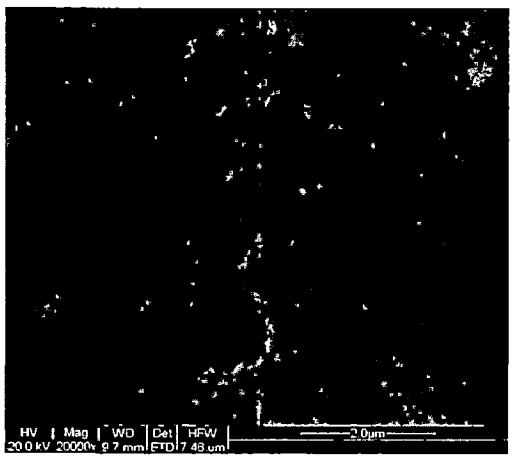

S-5

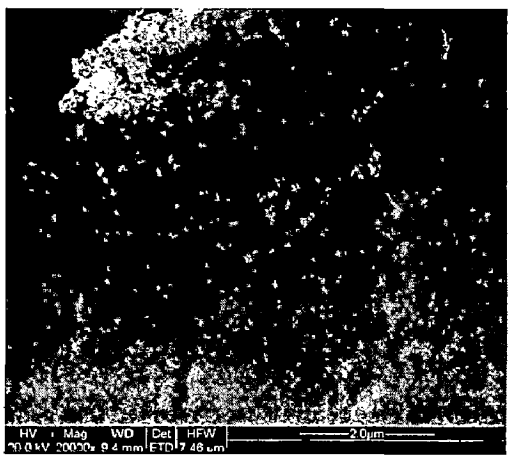

S-6

Fig.3.14. FE-SEM images of silver — sol-gel alumina nanocomposites before calcination. For details on samples, see Table 2.1 on p. 12.

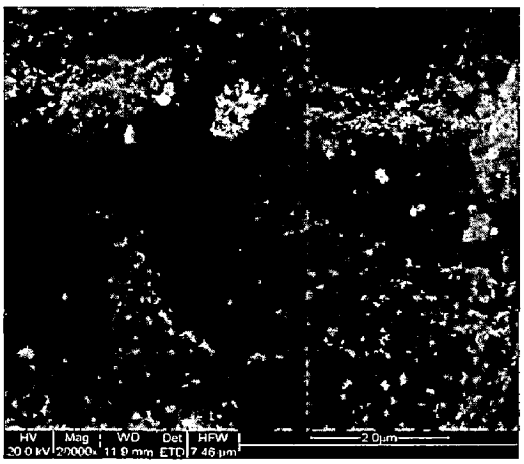

S-1

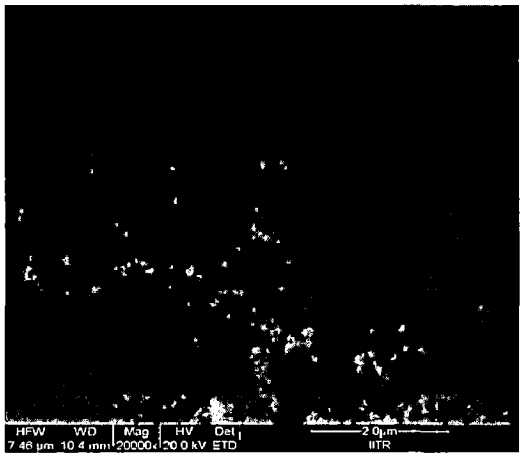

S-2

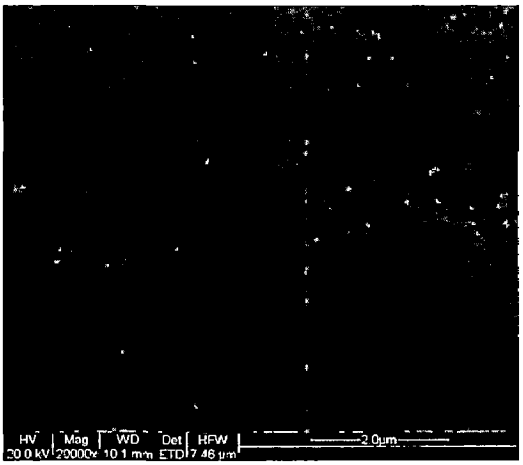

S-3

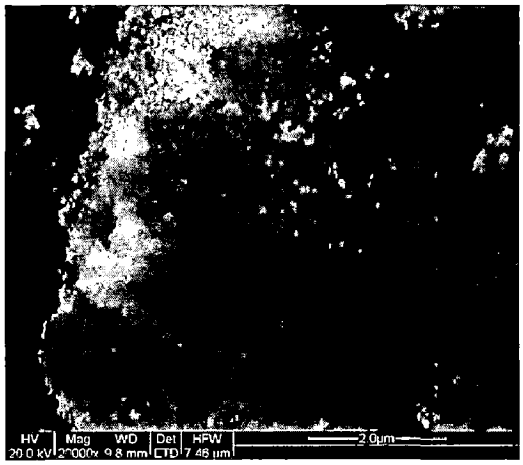

S-4

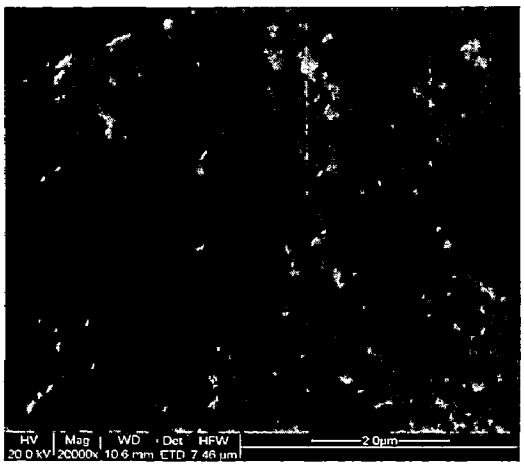

S-5

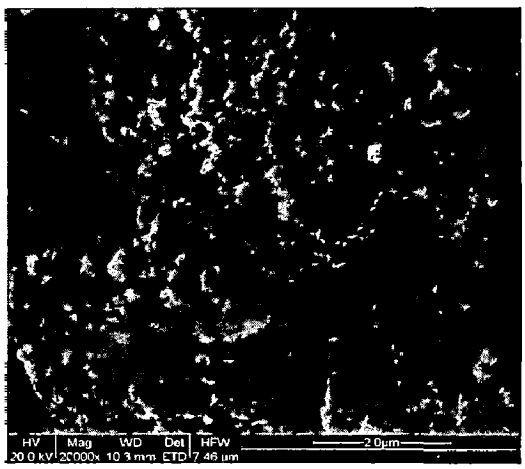

S-6

Fig.3.15. FE-SEM images of silver — sol-gel alumina nanocomposites after calcination.

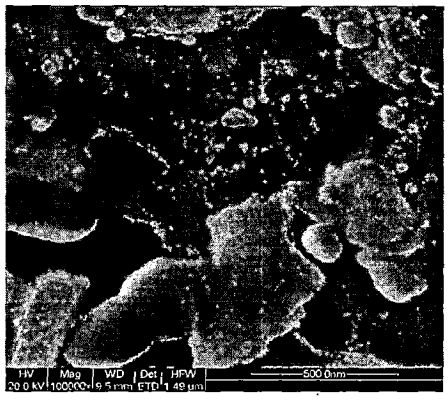

S-7

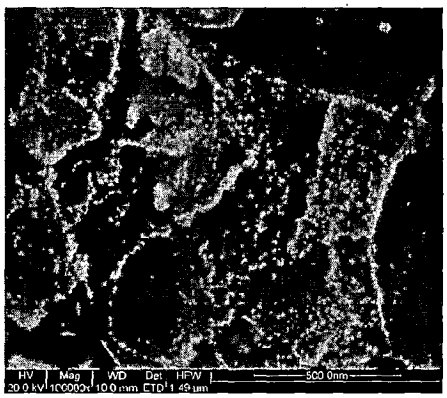

S-8

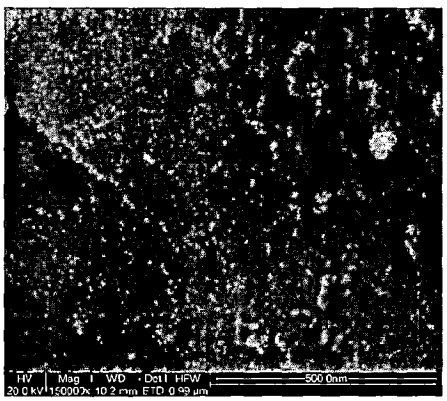

S-9

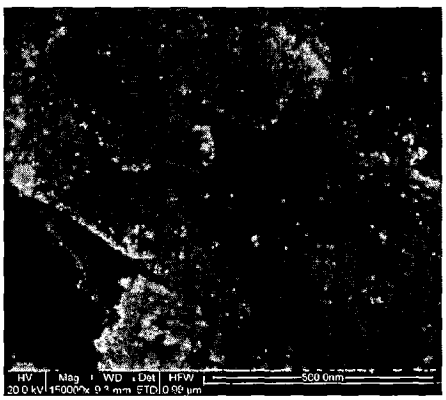

S-10

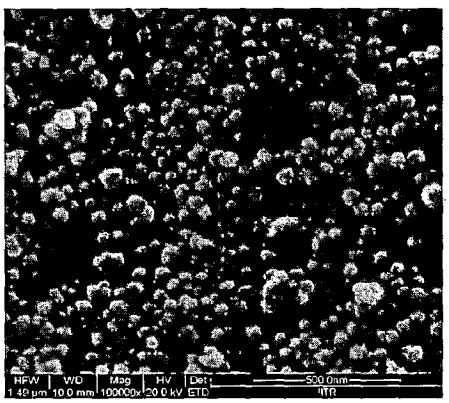

S-11

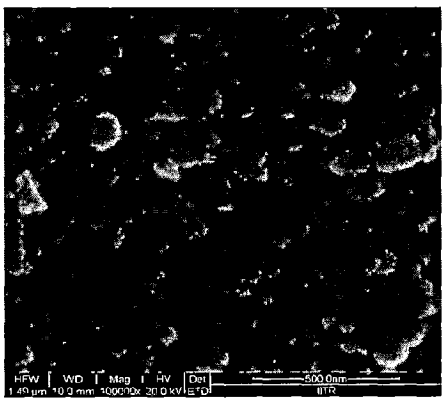

S-12

Fig.3.16. FE-SEM images of silver — commercial alumina nanocomposites before calcination.

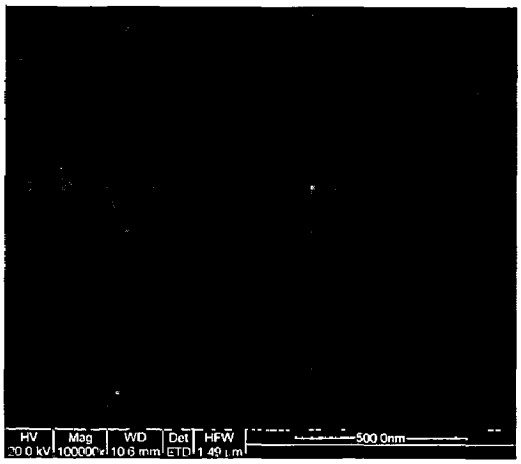

S-7

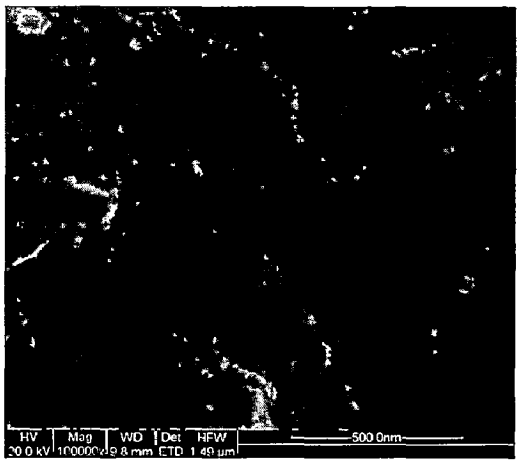

S-8

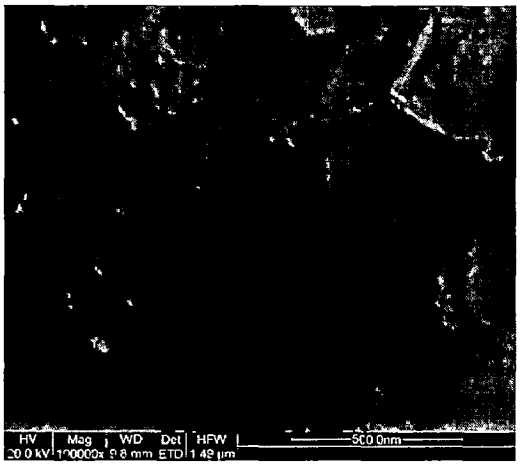

S-9

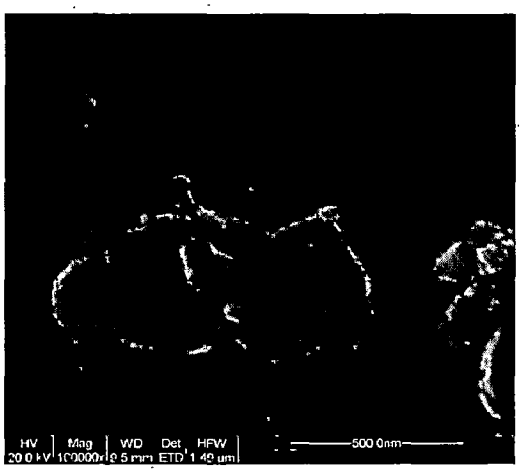

S-10

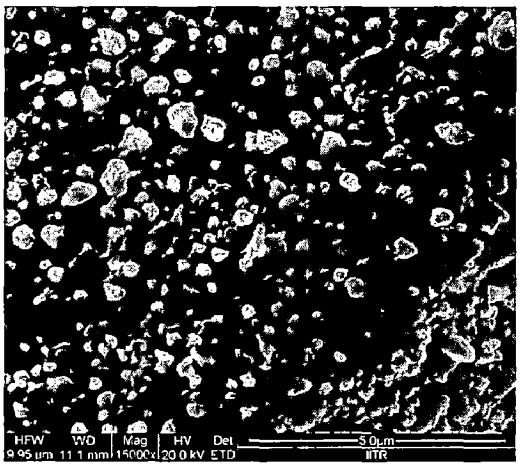

S-11

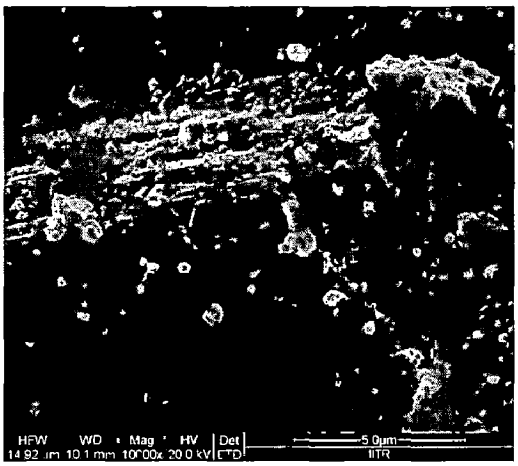

S-12

Fig.3.17. FE-SEM images of silver — commercial alumina nanocomposites after calcination.

Table 3.9. EDXA results of the silver-alumina nanocomposites before and after calcination.

Sample	Before Calcination				After Calcination			
	% C	% O	% Al	% Ag	% C	% O	% Al	% Ag
S1	44.5	11.1	21.6	22.7	7.3	21.4	43.0	28.3
	49.7	13.0	21.0	16.3	4.6	20.0	46.7	28.6
	37.7	7.5	29.8	25.0	9.5	20.0	37.8	32.7
S2	56.9	9.8	12.7	20.5	12.3	17.7	23.6	46.3
	51.9	11.9	13.3	22.9	13.7	15.9	22.0	48.4
	46.8	4.8	16.7	31.6	12.0	19.0	23.1	45.4
S3	30.1	8.8	17.5	43.5	20.2	32.1	40.0	7.6
	-	-	-	-	23.8	9.0	37.0	30.0
	-	-	-	-	-	-	-	-
S4	45.0	12.5	10.9	31.5	54.3	17.6	10.6	17.4
	44.6	14.0	11.7	29.6	-	-	-	-
	30.4	14.0	12.7	33.7	-	-	-	-
S5	42.9	15.0	28.1	13.9	50.3	19.6	24.6	5.5
	42.5	17.2	23.0	17.3	52.4	20.0	23.2	4.4
	-	-	-	-	-	-	-	-
S6	32.6	28.9	31.3	7.8	4.6	22.6	40.9	32.0
	29.9	29.0	36.1	5.0	4.8	4.8	39.9	33.5
	25.9	32.7	38.0	3.5	7.2	7.2	31.8	34.5
S7	3.0	9.1	18.8	69.1	4.0	6.0	5.9	84.0
	0.5	2.3	5.1	92.0	5.5	22.3	33.4	38.7
	-	-	-	-	-	-	-	-
S8	5.0	23.0	43.4	28.6	5.4	25.0	34.1	35.5
	2.4	22.4	45.0	30.0	3.5	15.3	21.0	60.1
	-	-	-	-	-	-	-	-
S9	7.7	14.7	32.0	45.5	7.0	19.4	31.0	42.7
	4.6	22.4	39.6	33.3	5.9	10.1	11.7	72.4
	-	-	-	-	54.7	7.2	2.8	35.3
S10	15.2	29.7	47.1	8.0	5.3	13.0	26.9	54.7
	17.9	22.3	50.8	9.0	7.7	18.5	28.0	45.7
	-	-	-	-	4.5	15.1	47.4	32.9
S11	9.5	15.3	50.1	25.0	18.4	22.7	30.4	28.6
	16.6	9.3	28.4	45.6	10.1	26.3	47.1	16.5
	26.4	19.0	24.0	30.5	16.3	12.3	18.8	52.6
S12	9.1	2.3	38.7	49.8	7.49	14.5	43.0	35.0
	21.0	11.3	22.0	45.8	6.49	3.5	36.2	53.8
	5.8	1.2	47.6	45.3	4.53	8.0	15.6	71.9

3.6. TEM Analysis

The TEM images were recorded for the sol-gel alumina (fig. 3.18), silver — sol-gel alumina nanocomposites (S-1, S-2 and S-6) (Figs 3.18, 3.19) and silver — commercial alumina nanocomposites (S-7, S-8 and S-12) (Fig. 3.21). The average particle size values of the silver nanoparticles were obtained for S-1, S-2 and S-6 samples in which the silver nanoparticles are not agglomerated. The average particle size values of silver nanoparticles in S-1, S-2 and S-6 sample are 8.17 ± 2.1, 23.6 ± 0.2, 8.86 ± 1.38, respectively. The particles size distributions of the silver nanoparticles are shown in the histograms (Fig. 3.20).

The TEM images indicate that the silver nanoparticles are finely dispersed on sol-gel alumina when compared to that on commercial alumina.

Fig.3.18. TEM image of sol-gel alumina after calcination.

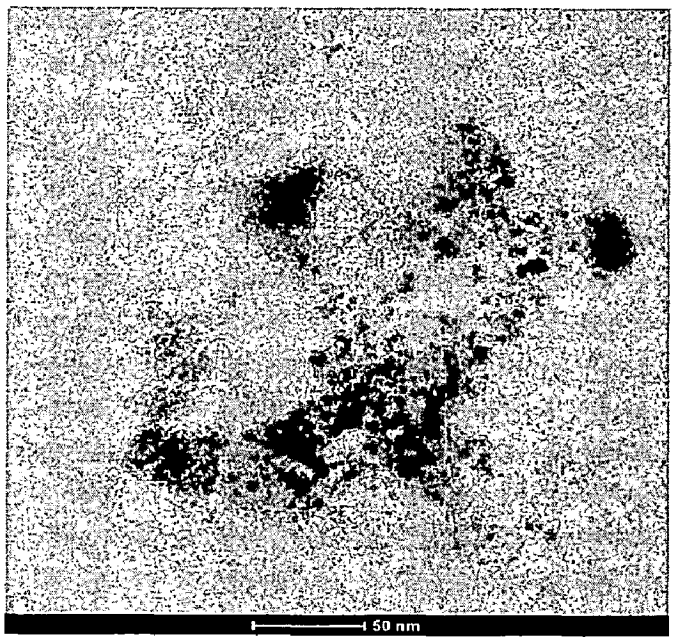

S-1

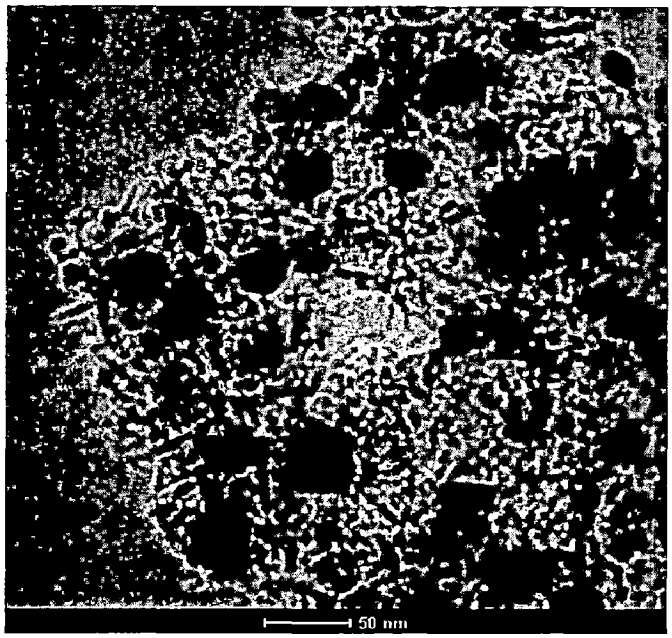

S-2

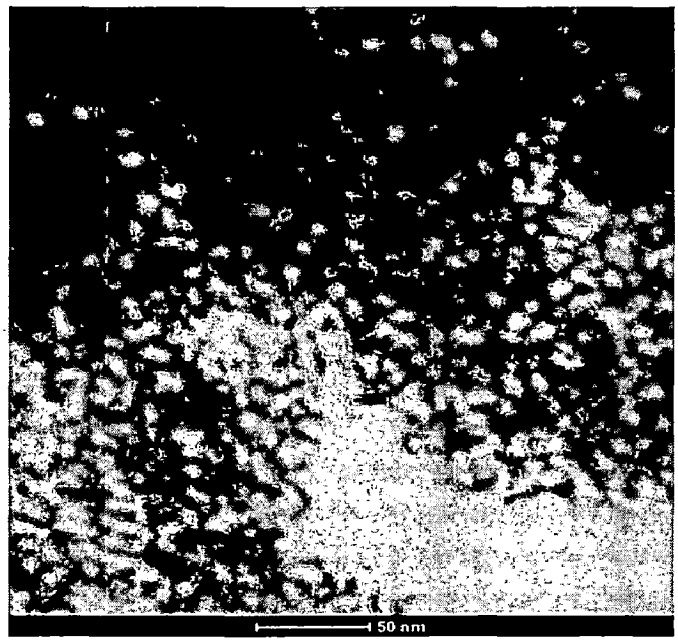

S-6

Fig.3.19. TEM images of silver — sol-gel alumina nanocomposites after calcination.

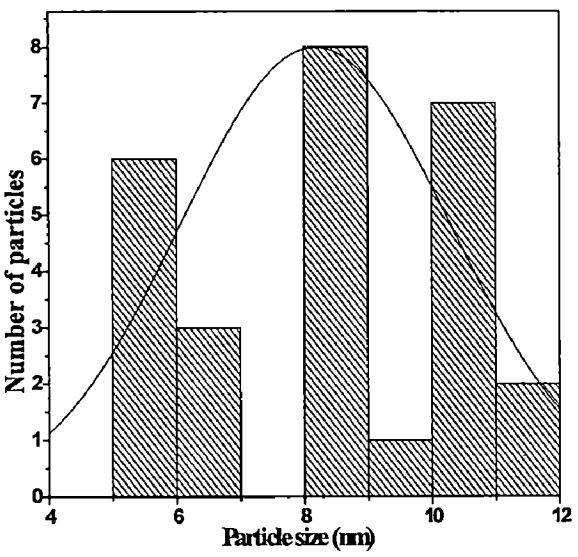

S-1

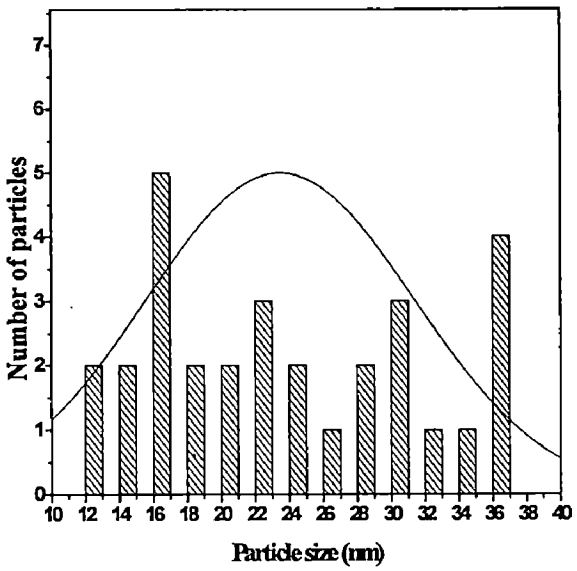

S-2

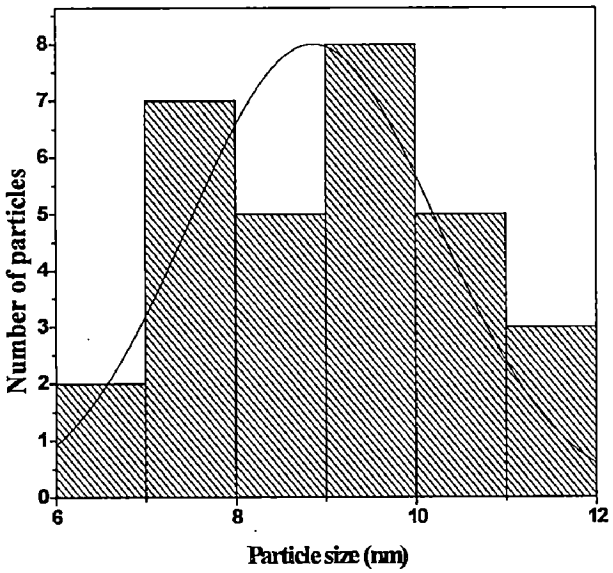

S-6

Fig.3.20. Particle size histograms of silver nanoparticles in silver — sol-gel alumina nanocomposites.

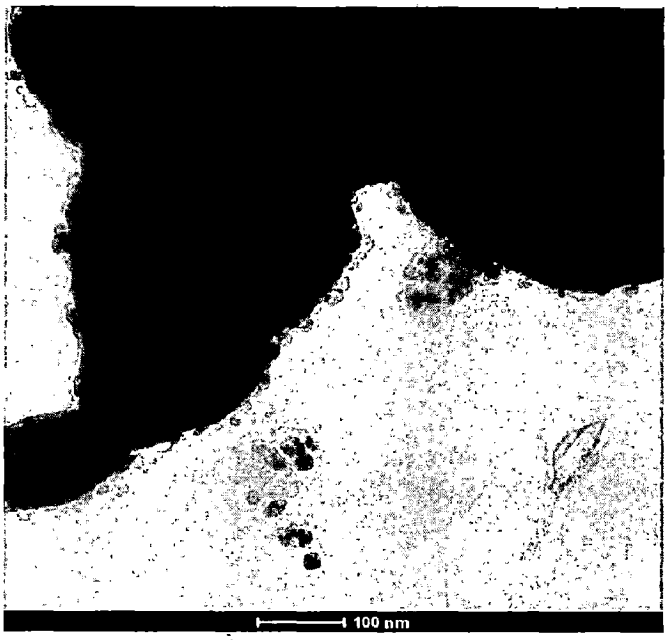

S-7

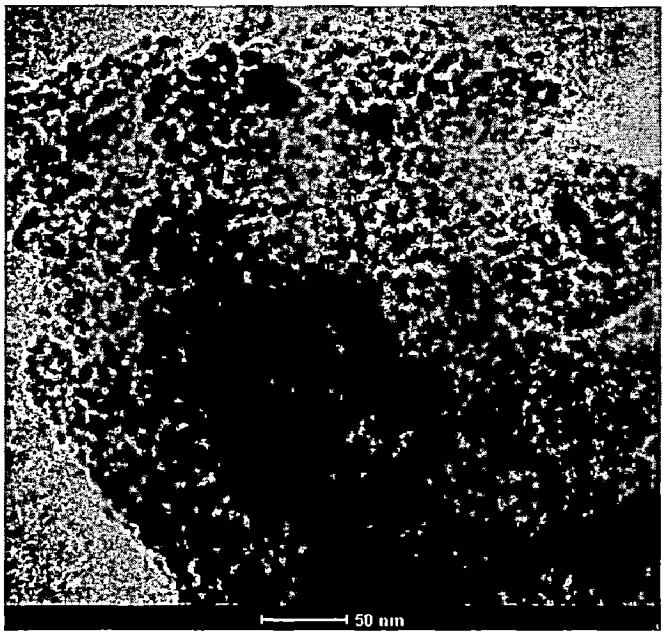

S-8

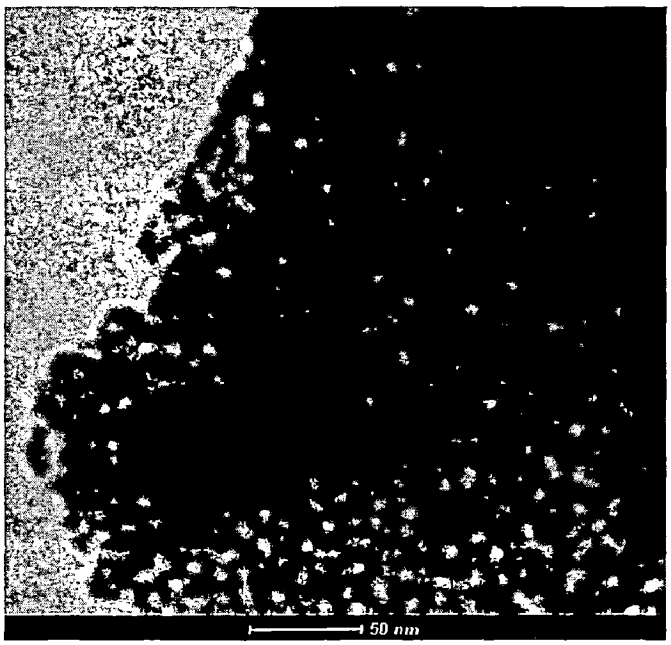

S-12

Fig.3.21. TEM images of silver — commercial alumina nanocomposites after calcination.

3.7. Diffuse Reflectance Spectral Studies

Diffuse reflectance spectra of Ag — alumina nanocomposites prepared using sol-gel alumina are shown in Fig. 3.22. All the Ag — sol-gel alumina nanocomposites show surface plasmon resonance (SPR) due to the presence of nanocrystalline silver. The intensity of SPR band is more when sol-gel alumina with calcination is used compared to that prepared using sol-gel alumina without calcination.

The Ag — commercial alumina nanocomposites do not show the characteristic SPR band for the nanocrystalline silver (Fig. 3.23).

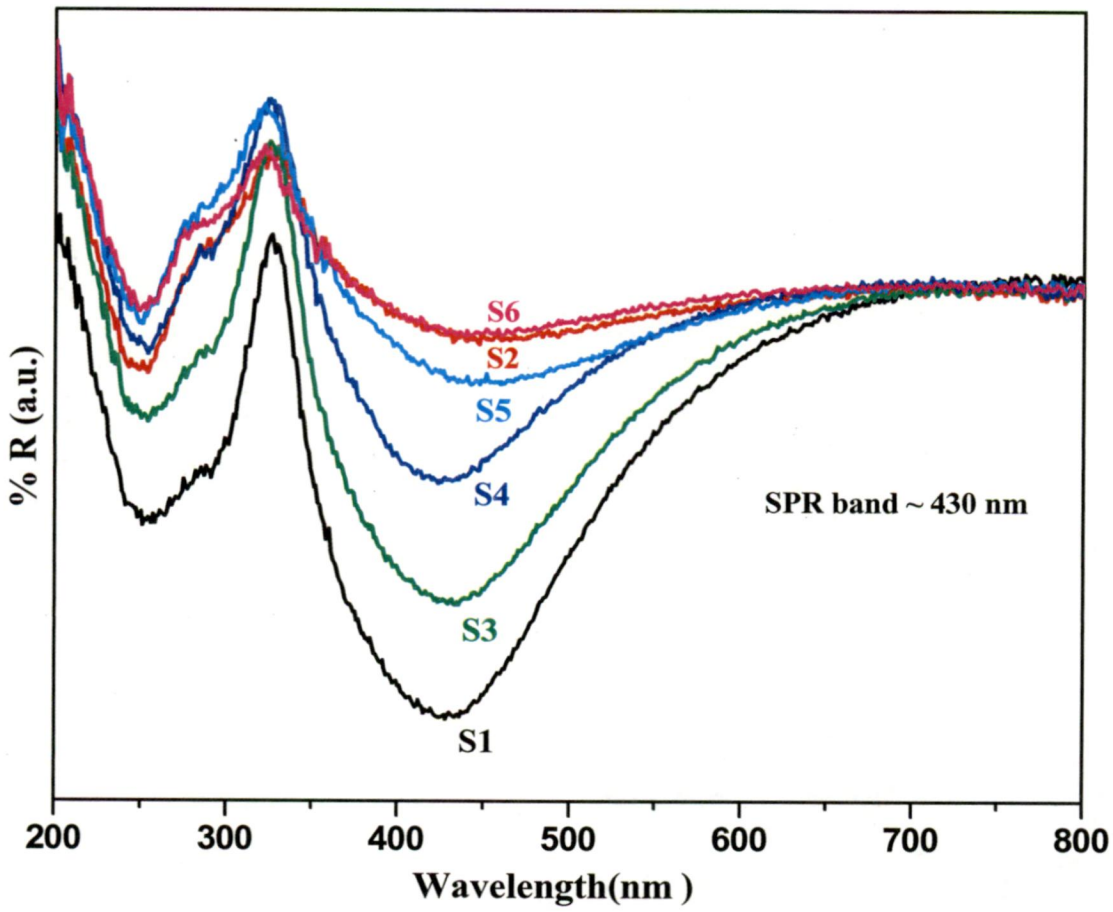

Fig.3.22. Diffuse reflectance spectra for the silver — sol-gel alumina nanocomposites.

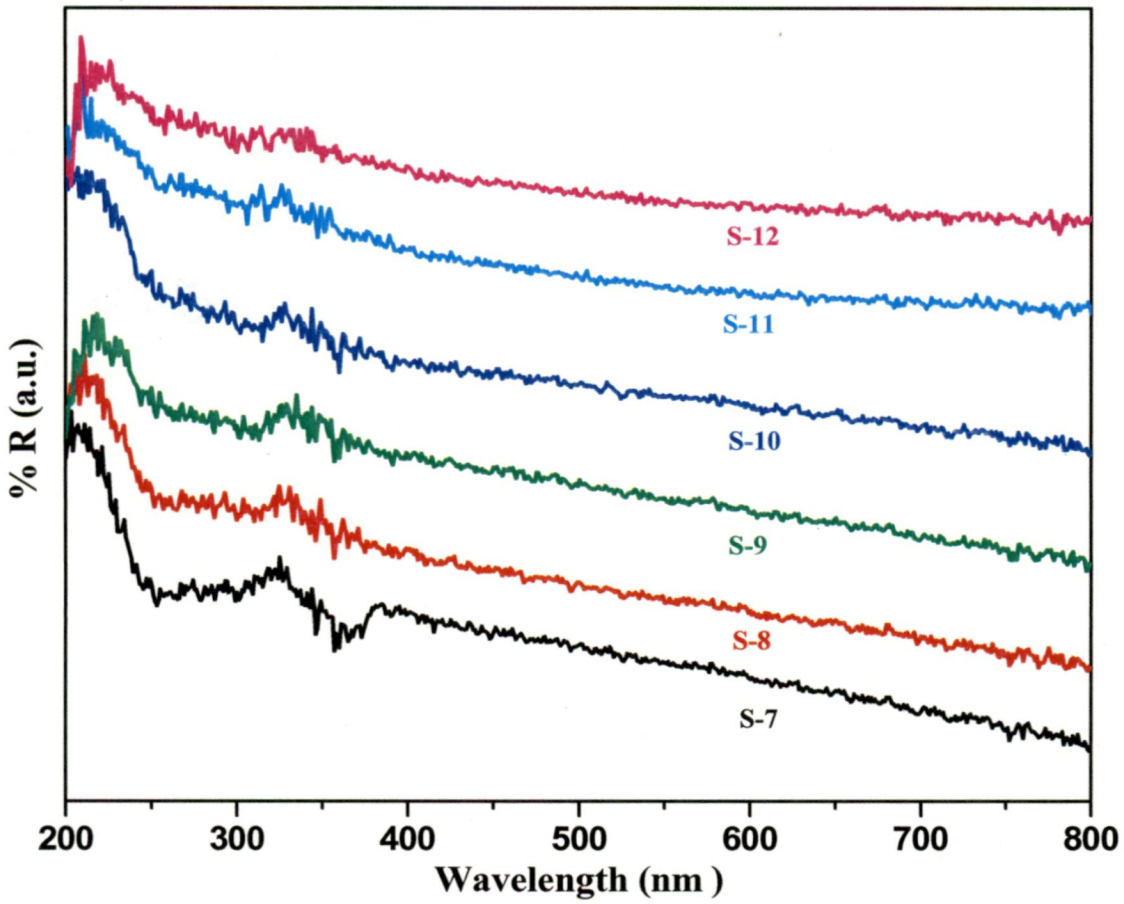

Fig.3.23. Diffuse reflectance spectra for the silver – commercial alumina nanocomposites.

3.8. Mechanism of Formation of Silver — alumina Nanocomposites

Aluminium isopropoxide is hydrolyzed by mixing with water to yield isopropyl alcohol and pseudoboehmite (AlO(OH)). Al_2O_3 forms upon dehydration of the pseudoboehmite phase (AlO(OH)) at 500 °C [32].

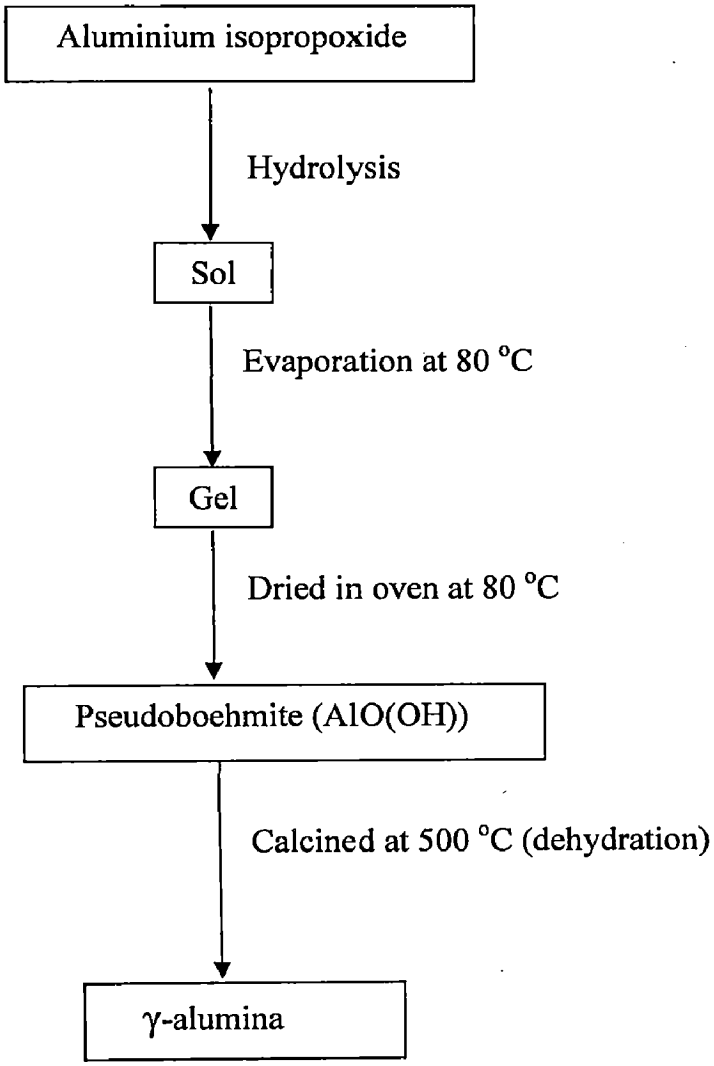

Fig.3.24. A schematic indicating the mechanism of formation of alumina nanoparticles

The reactions involved are given below.

$$Al(OR)_3 + H_2O \longrightarrow Al(OR)_2(OH) + ROH \quad \text{----------(I)}$$

$$Al(OR)_2(OH) + H_2O \longrightarrow AlO(OH) + 2\,ROH \quad \text{---------- (II)}$$

$$2\,AlO(OH) \longrightarrow Al_2O_3 + H_2O \quad \text{---------- (III)}$$

Pseudo-boehmite phase γ-alumina nanoparticles

Thermal decomposition of silver acetate may be represented as follows [64]:

$$2\,CH_3COOAg \xrightarrow{200\text{-}225\ ^\circ C} 2\,CH_3COOH\,(g) + CO_2\,(g) + H_2\,(g) + C + 2Ag^\circ$$

3.9. Catalytic Activity Studies

The catalytic activity of the synthesized Ag — alumina nanocomposites was tested for the reduction of 4-nitrophenol (4-NP) to 4-aminophenol (4-AP) by sodium borohydride as the reducing agent. To about 50 mL of aqueous solution of 4-nitrophenol (0.1 mmol), 50 mL of freshly prepared aqueous solution of $NaBH_4$ (0.529 mol/L) was added. About 20 mg of the catalyst (silver — alumina nanocomposites) was then added to the reaction mixture and the contents were kept for constant stirring at room temperature. The complete reduction of 4-nitrophenol (yellow coloured solution) was indicated by the decolorization of the solution due to the formation of 4-aminophenol. The reduction of 4-nitrophenol with $NaBH_4$ was also carried out in the absence of the catalyst. The time required for the complete reduction of 4-nitrophenol when different nanocomposites were used as catalysts is given in Table 3.10.

Table 3.10. Time required for the complete reduction of 4-nitrophenol to 4-aminophenol in the presence of different silver — alumina nanocomposites as catalysts.

Samples	Time required for the complete reduction (sec)
P-NP + $NaBH_4$ (without any catalyst)	No reduction
P-NP + $NaBH_4$ + Pure Ag nanoparticles	1320
P-NP + $NaBH_4$ + Pure sol-gel alumina	No reduction
P-NP + $NaBH_4$ + Pure commercial alumina	No reduction
S-1	15
S-2	6
S-3	20
S-4	5
S-5	6
S-6	4
S-7	240
S-8	480
S-9	480
S-10	240
S-11	1020
S-12	540

On the basis of reported reduction mechanism [48, 51, 54, 62], two processes occur during the reduction of 4-nitrophenol by $NaBH_4$ in the presence of catalyst (silver — sol-gel/commercial alumina nanocomposites): The first process is the adsorption of 4-nitrophenolate ions and also BH_4^- on the surface of the catalyst by chemical interaction (chemisorption). After adsorption, then the second process starts in which Ag nanoparticles help with the electron transfer from BH_4^- ions (donor) to the NO_2 group (acceptor) to form 4-aminophenolate ions. Desorption of the 4-aminophenolate ions occurs immediately from the catalyst surface as shown in Fig.3.25

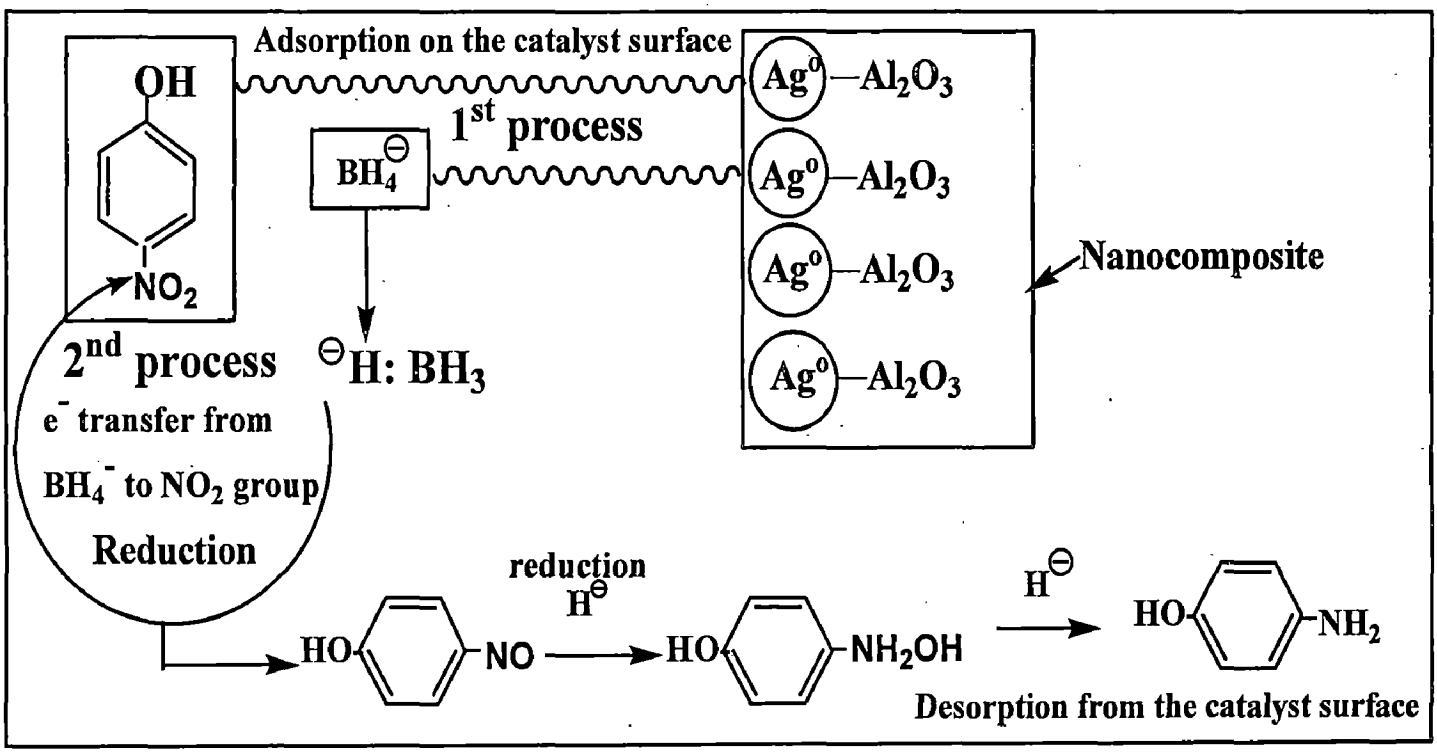

Fig.3.25. A schematic indicating the mechanism for the reduction of 4-nitrophenol to 4-aminophenol in the presence of silver — alumina nanocomposites.

From the Table 3.10, it can be concluded that the reduction of 4-nitrophenol does not take place in the absence of catalyst. Also, reduction of 4-nitrophenol does not occur when pure sol-gel alumina or commercial alumina is used as the catalyst. The silver — sol-gel alumina nanocomposites (time of reduction: 4 to 20 sec) and the silver — commercial alumina nanocomposites (time of reduction: 240 to 1020 sec) act as better catalysts compared to pure Ag nanoparticles (time of reduction: 1320 sec). This is attributed to the higher surface area of sol-gel alumina (525.64 m^2 g^{-1}) compared to commercial alumina (101.89 m^2 g^{-1}). Silver nanoparticles are highly dispersed on the surface of alumina and hence the catalytic activity of nanocomposites is greater than that due to pure silver nanoparticles (i.e. without alumina).

The catalytic activity of silver — alumina nanocomposites increases with the decrease of Ag concentration in the silver— sol-gel alumina nanocomposites in the following order: Ag — sol-gel Al_2O_3 (S-6, 0.25:1) >Ag — sol-gel Al_2O_3 (S-4, 0.5:1) > Ag — sol-gel Al_2O_3 (S-1, 1:1).

CHAPTER 4

SUMMARY

CHAPTER 4

SUMMARY

Silver — alumina nanocomposites have been successfully synthesized by a simple thermal decomposition method. Two types of alumina, i.e. sol-gel and commercial (with / without calcination) have been employed for the synthesis of the nanocomposites. The silver-alumina nanocomposites were characterized using a variety of analytical techniques, it was concluded that the silver nanoparticles are well dispersed on the surface of sol-gel alumina when compared to commercial alumina. Hence sol-gel alumina acts as a better supporting material in the preparation of the silver – alumina nanocomposites. From the SEM and TEM results, it was found that less agglomeration of silver nanoparticles is observed when lower concentration of silver acetate is employed during the thermal decomposition. Catalytic activity of the silver — alumina nanocomposites was investigated by the reduction of 4-nitrophenol (4-NP) to 4-aminophenol (4-AP). On the basis of catalytic activity studies, it was concluded that the nanocomposites act as better catalysts compared to pure silver nanoparticles. Also, the silver — sol-gel alumina nanocomposites show better catalytic activity towards the reduction of 4-NP compared to the silver — commercial alumina nanocomposites due to the fine dispersion of silver nanoparticles on the surface of sol-gel alumina. The catalytic activity of nanocomposites increases with the decrease in concentration of the silver acetate employed during the preparation of the silver — sol-gel alumina nanocomposites.

CHAPTER 5

FUTURE PROSPECTS

CHAPTER 5

FUTURE PROSPECTS

Silver — sol-gel / commercial alumina nanocomposites may be used as for the catalytsts reactions such as degradation of organic dyes in waste water (e.g. methyl orange), partial oxidation of ethylene to ethylene oxide and hydrosulphurization of dibenzothiophene. Also, the nanocomposite may be tested for anti-bacterial activity.

REFERENCES

REFERENCES

1. Gunter Schmid, Nanoparticles: From Theory to Application, WILEY-VCH Verlag GmbH & Co. KGaA, Weinheim, 2004

2. P. M. Ajayan, L. S. Schadler, P. V. Braun, Nanocomposite Science and Technology, Wiley-VCH, Weinheim, 2003

3. S. J. Son, X. Bai, A. Nan, H. Ghandehari, S. B. Lee, Journal of Controlled Release, 114, 2006, 143-152

4. Z. Zhang, D. L. Chen, Scripta Materialia 54, 2006, 1321-1326

5. L. M. Hamming, R. Qiao, P. B. Messersmith, L. C. Brinson, Composites Science and Technology, 69, 2009, 1880-1886

6. L. Schanghua, L. M. Meng, S. T. Muhammet, D. K. Kim, M. Muhammed, Nano Reviews, 1, 2010, 5214/1-5214/19

7. S. M. Choi, H. Awaji, Science and Technology of Advanced Materials, 6, 2005, 2-10

8. J. S. Moya, S. L. Esteban, C. Pecharroman, Progress in Materials Science, 52, 2007, 1017-1090

9. M. Sternitzke, Journal of the European Ceramic Society, 17, 1997, 1061-1082

10. F. Misjak, P.B. Barna, A.L. Toth, T. Ujvari, I. Bertoti, G. Radnoczi, Thin Solid Films, 516, 2008, 3931-3934

11. R. Seoudi, A. B. E. Bailly, W. Eisa, A. A. Shabaka, S. I. Soliman, R. K. A. E. Hamid, R. A. Ramadan, Journal of Applied Sciences Research, 8, 2012, 658-667

12. H. Zhang, Y. Sun, J. Wang, J. Zhang, H. Zhang, H. Zhou, D. Song, Biosensors and Bioelectronics, 34, 2012, 137-143

13. C.Yang, X. chunxiang, X. Wang, Langmuir, 28, 2012, 4580-4585

14. J. Zeng, P. K. Shen, S. Lu, Y. Xiang, L. Li, R. D. Marco, S. P. Jiang, Journal of Membrane Science, 92 – 101, 2012, 397-398

15. J. Gaume, C. T. Gueho, S. Cros, A. Rivaton, S. Therias, J. L. Gardette, Solar Energy Materials and Solar Cells, 99, 2012, 240-249

16. I. Morjan, F. Dumitrache, R. Alexandrescu, C. Fleaca, R. Birjega, C.R. Luculescu, I. Soare, E. Dutu, G. Filoti, V. Kuncser, G. Prodan, N. C. Popa, L. Vekas, Advanced Powder Technology, 23, 2012, 88-96

17. C. H. Pelisson, Lucas L. L. R. Vono, C. Hubert, A. D. Nowicki, L. M. Rossi, A. Roucoux, Catalysis Today, 183, 2012, 124-129

18. I. Maksimenko, P. J. Wellmann, Thin Solid Films, 520, 2011, 1341-1347

19. M. Zhang, K. Zhang, B. D. Gusseme, W. Verstraete, Water Research, 46, 2012, 2077-2087

20. S. Pande, A. Saha, S. Jana, S. Sarkar, M. Basu, M. Pradhan, A. K. Sinha, S. Saha, A. Pal, and T. Pal, Organic Letters,10, 2008, 5179-5181

21. A. D. Gledhill, D. Li, T. Mroz, L. M. Goldman, N. P. Padture, Acta Materialia, 60, 2012, 1570-1575

22. Y. A. Krutyakov, A. A. Kudrinskiy, A. Y. Olenin, G. V. Lisichkin, Russian Chemical Reviews, 77, 2008, 233-257

23. Y. Kim, S. M. Lee, C. S. Park, S. I. Lee, M. Y. Lee, Applied Physics Letters, 71, 1997, 3604-3606

24. E. P. Gusev, M. Copel, E. Cartier, I. J. R. Baumvol, C. Krug, Applied Physics Letters, 76, 2000, 176-178

25. A. P. Minardi, O. Marty, C. Bovier, C. Garapon, J. Mugnier. Optical Materials, 16, 2001, 9-13

26. M. I. F. Macedo, C. C. Osawa, C. A. Bertran, Journal of Sol-Gel Science and Technology 30, 2004, 135-140

27. T. Bala, G. Armstrong, F. Laffir, R. Thornton, Journal of Colloid and Interface Science, 356, 2011, 395-403

28. C. L. Lu, J. G. Lv, L. Xu, X. F. Guo, W. H. Hou, Y. Hu, H. Huang, Nanotechnology, 20, 2009, 215604/1-215604/9

29. F. Rashidi, E. Limab, H. Rashidi, A. Rashidi, A. Guzman, Applied Catalysis A, 417-418, 2012, 129-136

30. B. Bora, N. Aomoa, R. K. Bordooi, D. N. Srivastava, H. Bhuyan, A. K. Das, M. Kakati, Current Applied Physics, 12, 2012, 880-884

31. C. Morterra, G. Magnacca, Catalysis Today, 27, 1996, 497-532

32. G. L. Teoh, K. Y. Liew, W. A. K. Mahmood, Journal of Sol-Gel Science Technology, 44, 2007, 177-186

33. Z. Hosseini, M. Taghizadeh, F. Yaripour, Journal of Natural Gas Chemistry, 20, 2011, 128-134

34. M. Akia, S. M. Alavi, M. Rezaei, Z. F. Yan, Microporous and Mesoporous Materials, 122, 2009, 72-78

35. Y. K. Park, E. H. Tadd, M. Zubris, R. Tannenbaum, Materials Research Bulletin, 40, 2005, 1506-1512

36. M. Crisan, M. Zaharescu, V. D. Kumari, M. Subrahmanyam, D. Crisan, N. Dragan, M. Raileanu, M. Jitianu, A. Rusu, G. Sadanandam, J. K. Reddy, Applied Surface Science, 258, 2011, 448-455

37. N. Lepot, M. K. V. Bael, H. V. D. Rul, J. D. Haen, R. Peeters, D. Franco, J. Mullens, Ceramics International, 34, 2008, 1971-1974

38. V. G. Pena, C. M. Alvarez, I. Diaz, M. Grande, T. Blasco, J. P. Pariente, Microporous and Mesoporous Materials, 80, 2005, 173-182

39. A. K. Patra, A. Dutta, A. Bhaumik, Journal of Hazardous Materials, 201-202, 2012, 170-177

40. T. Sato, S. Goto, Q. Tang, S. Yin, Journal of Materials Science, 43, 2008, 2247-2253

41. H. J. Tang, F. Q. Wu, H. L. Wang, Y. H. Wei, Q. S. Li, Optik, 119, 2008, 134-138

42. Y. H. Yeom, M. Li, W. M. H. Sachtler, E. Weitz, Journal of Catalysis, 238, 2006, 100-110

43. K. I. Shimizu, A. Satsuma, T. Hattori, Applied Catalysis B: Environmental, 25, 2000, 239-247

44. J. N. Solanki, Z. V. P. Murthy, Industrial and Engineering Chemistry Research, 50, 2011, 7338-7344

45. Y. S. Cho, B. U. Lee, K.H. Oh, Journal of Chemical Technology and Biotechnology, 83, 2008, 1211-1217

46. F. D. M. Sikkema, J. A. M. de Bont, Applied Microbiology and Biotechnology, 42, 1994, 499-507

47. R. Dillert, M. Brandt, I. Fornefett, U. Siebers, D. Bahnemann, Chemosphere, 30, 1995, 2333-2341

48. S. Kundu, M. Mandal, S. K. Ghosh, T. Pal, Journal of Colloid and Interface Science, 272, 2004, 134-144

49. G. Dang, Y. Shi, Z. Fu, W. Yang, Journal of Colloid and Interface Science, 369, 2012, 170-178

50. S. Xiao, W. Xu, H. Ma, X. Fang, RSC Advances, 2, 2012, 319-327

51. P. Liu, M. Zhao, Applied Surface Science, 255, 2009, 3989-3993

52. A. R. Kiasat, R. Mirzajani, F. Ataeian, M. F. Mehrjardi, Chinese Chemical Letters, 21, 2010, 1015-1019

53. N. Pradhan, A. Pal, T. Pal, Colloids and Surfaces A: Physicochemical Engineering Aspects, 196, 2002, 247-257

54. Q. Zhou, G. Qian, Y. Li, G. Zhao, Y. Chao, J. Zheng, Thin Solid Films, 516, 2008, 953-956

55. X. She, M. F. Stephanopoulos, Journal of Catalysis, 237, 2006, 79-93

56. M. Haji, T. Ebadzadeh, M. H. Amin, M. Kazemzad, T. Talebi, Ceramics International, 38, 2012, 867-870

57. S. Bhattacharyya, A. Gabashvili, N. Perkas, A. Gedanken, Journal of Physical Chemistry C, 111, 2007, 11161-11167

58. P. N. R. Kishore, P. Jeevanandam, Journal of Nanoscience and Nanotechnology, 11, 2011, 3445-3453

59. F. Mirjalili, M. Hasmaliza, L. C. Abdullah, Ceramics International, 36, 2010, 1253-1257

60. B. D. Cullity, S. R. Stock, 'Elements of X-ray Diffraction', Prentice Hall, 2001

61. M. S. Ghamsari, Z. A. S. Mahzar, S. Radiman, A.M. A. Hamid, S. R. Khalilabad, Materials Letters, 72, 2012, 32-35

62. S. K. Ghosh, M. Mandal, S. Kundu, S. Nath, T. Pal, Applied Catalysis A, 268, 2004, 61-66

63. M. D. Judd, B. A. Plunkett, M. I. Pope, Journal of Thermal Analysis, 6, 1974, 555-563

64. M. A. Mahmoud, F. Saira, M. A. E. Sayed, Nano Letters, 10, 2010, 3764-3769

65. M. Coskun, G. H. Jaffari, S. Manzoor, M. Korkmaz, S.I. Shah, Journal of Magnetism and Magnetic Materials, 322, 2010, 1731-1735

66. J. A. Sanchez, B. L. Rivas, S. A. Pooley, L. Basaez, E. Pereira, I. P. Paintrand, C. Bucher, G. Royal, E. S. Aman, J. C. Moutet, Electrochimica Acta, 55, 2010, 4876-4882

67. U. Pal, J. G. Serrano, G. C. Segura, N. Koshizaki, T. Sasaki, S. Terahuchi, Solar Energy Materials and Solar Cells, 81, 2004, 339-348

68. D. Ortega, J. S. Garitaonandia, C. B. Solano, M. Dominguez, Sensors and Actuators A, 142, 2008, 554-560

69. B. S. Kadua, Y. D. Sathea, A. B. Inglea, R. C. Chikatea, K. R. Patil, C. V. Rode, Applied Catalysis B: Environmental, 104, 2011, 407-414

70. C. S. Chou, R. Y. Yang, C. K. Yeh, Y. J. Lin, Powder Technology, 194, 2009, 95-105

71. L. S. Sales, P.A. R. Dutenhefner, D. L. Nunes, N. D. S. Mohallem, E. V. Gusevskaya, E. M. B. Sousa, Materials Characterization, 50, 2003, 95-99

72. J. A. Nuetzel, C. J. Unrau, R. Indeck, R. L. Axelbaum, Proceedings of the Combustion Institute, 32, 2009, 1871-1877

PUBLICATION

Ravi Kant Sharma and P. Jeevanandam, "A Novel Thermal Decomposition Approach for the Synthesis of Silver-Alumina Nanocomposites", submitted to *Journal of Alloys and Compounds.*